PRODUCTION OF BIO-OLEFINS FROM OLEIC ACID

VIA OXIDATIVE DEHYDROGENATION USING VANADIUM OXIDES/SBA-15 CATALYSTS

Miss Nattaporn Chaidherasuwet

A Thesis Submitted in Partial Fulfillment of the Requirements

for the Degree of Master of Science in Petrochemistry and Polymer Science

Field of Study of Petrochemistry and Polymer Science

FACULTY OF SCIENCE

Chulalongkorn University

Academic Year 2021

การผลิตโอเลฟินชีวภาพจากกรดโอเลอิก
ผ่านออกซิเดทีฟดีไฮโดรจิเนชันโดยตัวเร่งปฏิกิริยาวาเนเดียมออกไซด์/เอสบีเอ-15

น.ส.ณัฐพร ชัยธีระสุเวท

วิทยานิพนธ์นี้เป็นส่วนหนึ่งของการศึกษาตามหลักสูตรปริญญาวิทยาศาสตรมหาบัณฑิต
สาขาวิชาปิโตรเคมีและวิทยาศาสตร์พอลิเมอร์ สาขาวิชาปิโตรเคมีและวิทยาศาสตร์พอลิเมอร์
คณะวิทยาศาสตร์ จุฬาลงกรณ์มหาวิทยาลัย
ปีการศึกษา 2564

Thesis Title	PRODUCTION OF BIO-OLEFINS FROM OLEIC ACIDVIA OXIDATIVE DEHYDROGENATION USING VANADIUM OXIDES/SBA-15 CATALYSTS
By	Miss Nattaporn Chaidherasuwet
Field of Study	Petrochemistry and Polymer Science
Thesis Advisor	Professor NAPIDA HINCHIRANAN, Ph.D.

Accepted by the FACULTY OF SCIENCE, Chulalongkorn University in Partial Fulfillment of the Requirement for the Master of Science

.... Dean of the FACULTY OF SCIENCE

(Professor POLKIT SANGVANICH, Ph.D.)

THESIS COMMITTEE

.... Chairman

(Professor Chawalit Ngamcharussrivichai, Ph.D.)

.... Thesis Advisor

(Professor NAPIDA HINCHIRANAN, Ph.D.)

.... Examiner

(Assistant Professor Duangamol Tungasmita, Ph.D.)

.... External Examiner

(Associate Professor Chanatip Samart, Ph.D.)

ณัฐพร ชัยธีระสุเวท : การผลิตโอเลฟินชีวภาพจากกรดโอเลอิกผ่านออกซิเดทีฟดีไฮโดรจิเนชันโดยตัวเร่ง
ปฏิกิริยาวาเนเดียมออกไซด์/เอสบีเอ-15. (PRODUCTION OF BIO-OLEFINS FROM OLEIC ACIDVIA
OXIDATIVE DEHYDROGENATION USING VANADIUM OXIDES/SBA-15 CATALYSTS) อ.ที่
ปรึกษาหลัก : ศ. ดร.นพิดา หิญชีระนันทน์

โอเลฟินสายโซ่ยาว (จำนวนอะตอมคาร์บอน ≥ 10) เป็นสารเคมีที่สำคัญในการผลิตสินค้าโภคภัณฑ์ใน
ชีวิตประจำวัน เช่น บรรจุภัณฑ์พลาสติก สารลดแรงตึงผิวและสารซักฟอกในผลิตภัณฑ์ทำความสะอาด รวมถึงสารเติม
แต่งในน้ำมันหล่อลื่นยานยนต์ อย่างไรก็ตามปัจจุบันโอเลฟินสายโซ่ยาวถูกสังเคราะห์ขึ้นในกระบวนการกลั่นน้ำมัน
ปิโตรเลียม ผ่านปฏิกิริยาเอทิลีนโอลิโกเมอไรเซชัน หรือการแตกตัวด้วยความร้อนของพาราฟินสายยาว ดังนั้นเพื่อ
ตอบสนองต่อนโยบายเศรษฐกิจชีวภาพ เศรษฐกิจหมุนเวียน และเศรษฐกิจสีเขียว ทำให้การสังเคราะห์โอเลฟินชีวภาพ
สายโซ่ยาวจากแหล่งทรัพยากรหมุนเวียนเป็นสิ่งที่น่าสนใจ โดยในงานวิจัยนี้มีวัตถุประสงค์เพื่อศึกษาความเป็นไปได้
ในการนำกรดโอเลอิก ซึ่งเป็นหนึ่งในองค์ประกอบกรดไขมันไม่อิ่มตัวในน้ำมันปาล์มมาใช้เพื่อผลิตโอเลฟินชีวภาพสาย
โซ่ยาวผ่านออกซิเดทีฟดีไฮโดรจิเนชันโดยใช้ตัวเร่งปฏิกิริยาวาเนเดียมออกไซด์บนตัวรองรับเอสบีเอ-15 ศึกษาอิทธิพล
ของตัวแปรต่าง ๆ ได้แก่ ปริมาณวาเนเดียมออกไซด์ (0.5, 1.0, 3.0, 5.0%โดยน้ำหนัก) อุณหภูมิในการทำปฏิกิริยา (
400-550 °ซ) เวลาในการดำเนินการ (2, 6, 8 ชั่วโมง) และความสามารถในการนำกลับมาใช้ซ้ำของตัวเร่งปฏิกิริยา
ต่อค่าการเปลี่ยนแปลงของกรดโอเลอิก และค่าการเลือกเกิดเป็นโอเลฟินชีวภาพที่อยู่ในรูปของผลิตภัณฑ์ของเหลว
พบว่าการทำปฏิกิริยาออกซิเดทีฟดีไฮโดรจิเนชันของกรดโอเลอิกโดยใช้ตัวเร่งปฏิกิริยาวาเนเดียมออกไซด์ 1.0 %โดย
น้ำหนัก ที่อุณหภูมิ 450 °ซ และใช้ระยะเวลาดำเนินการ 2 ชั่วโมง ให้ค่าการเปลี่ยนแปลงของกรดโอเลอิกมากที่สุด
(83.7%) ในขณะที่ตัวเร่งปฏิกิริยาที่มีวาเนเดียมออกไซด์ที่ 0.5 %โดยน้ำหนัก ให้ค่าการเลือกเกิดเป็นโอเลฟินชีวภาพ
สายโซ่ยาวมากที่สุด (44.6%) โดยมีจำนวนคาร์บอนอะตอมในโครงสร้างตั้งแต่ 7-17 อะตอม อย่างไรก็ตามการเพิ่ม
อุณหภูมิของปฏิกิริยาให้สูงขึ้นเป็น 550 °ซ สนับสนุนการเกิดแอโรมาไทเซชันทำให้เกิดสารประกอบแอโรมาติกถึง
25.4% นอกจากนี้การใช้ระยะเวลาดำเนินการที่มากเกินไป (6-8 ชั่วโมง) และ การนำกลับมาใช้ซ้ำมากกว่า 1 รอบ
ส่งผลให้ประสิทธิภาพของตัวเร่งปฏิกิริยาลดลง อันเนื่องมาจากโครงสร้างของตัวเร่งปฏิกิริยาบางส่วนถูกทำลายลง
และเกิดการสะสมของโค้กที่เพิ่มขึ้น

| สาขาวิชา | ปิโตรเคมีและวิทยาศาสตร์พอลิเมอร์ | ลายมือชื่อนิสิต .... |
| ปีการศึกษา | 2564 | ลายมือชื่อ อ.ที่ปรึกษาหลัก .... |

Nattaporn Chaidherasuwet : PRODUCTION OF BIO-OLEFINS FROM OLEIC ACIDVIA OXIDATIVE DEHYDROGENATION USING VANADIUM OXIDES/SBA-15 CATALYSTS. Advisor: Prof. NAPIDA HINCHIRANAN, Ph.D.

Long-chain olefins ($\geq$C10) are important commodity chemicals, which are primarily used to manufacture everyday products such as plastic packaging, surfactants and detergents in cleaning products, and lubricant oil additives. However, the long-chain olefins are currently synthesized from the petroleum refining process via ethylene oligomerization or thermal cracking of long-chain paraffins. To support the Bio-Circular-Green Economy (BCG) model, the direct synthesis of olefins from renewable feedstocks has become an attractive route to promote overall sustainability. The objective of this research was to study the possibility to transform oleic acid (OA), one of the unsaturated fatty acids in palm oil, to produce the long-chain bio-olefins via oxidative dehydrogenation (ODH) using an nV_xO_y/SBA-15 catalyst. The effects of various parameters such as vanadium content (0.5, 1.0, 3.0, and 5.0 wt%), reaction temperature (400-550 °C), processing time (2, 6, 8 h), and reusability of the catalyst on the OA conversion and the selectivity to olefins in the liquid and gaseous products was investigates. It was found that the ODH of OA using 1.0%V_xO_y/SBA-15 catalyst carried on at 450 ^{o}C for 2 h provided the best OA conversion (83.7%), whereas the 0.5%V_xO_y/SBA-15 catalyst obtained the high selectivity to long-chain olefins with carbon atoms in the range of C_7-C_{17} (44.6%). However, the higher reaction temperature at 550 ^{o}C promoted the aromatization for producing 25.4% of aromatic compounds. Moreover, the long-time process (6-8 h) and catalyst regeneration above 1st cycle decreased the catalyst performance due to the catalyst's structure collapse and increases in coke formation, respectively.

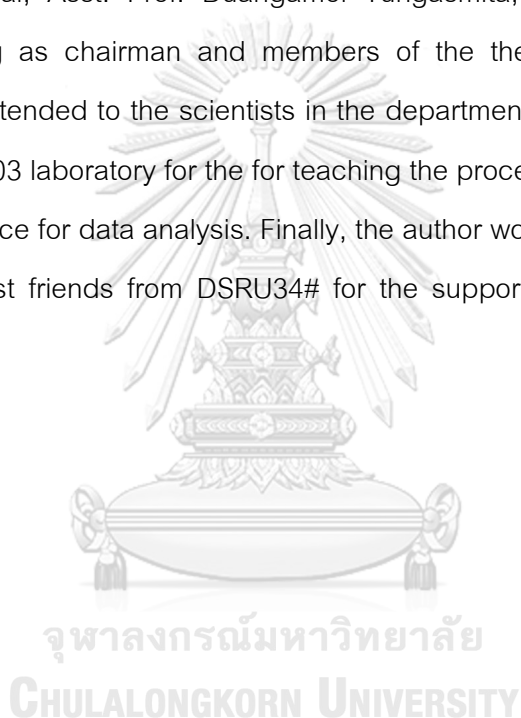Field of Study: Petrochemistry and Polymer Science

Academic Year: 2021

Student's Signature ....

Advisor's Signature ....

ACKNOWLEDGEMENTS

Nattaporn Chaidherasuwet

จุฬาลงกรณ์มหาวิทยาลัย
CHULALONGKORN UNIVERSITY

TABLE OF CONTENTS

TABLE OF CONTENTS

FIGURE OF CONTENTS

CHAPTER I

INTRODUCTION

1.1   Background and motivation

According to the Sustainable Development Goals (SDGs), oleochemicals is one of the green chemical species mainly derived from renewable resources including the natural products such as vegetable or animal oils. Basically, oleochemicals are produced from triglycerides obtained from vegetable oils and natural fats via hydrolysis or transesterification towards fatty acids and glycerin or methyl esters used in many applications such as pharmaceuticals, food, soap, rubber, adhesives, glues, greases and lubricants, paints, coatings, detergents, textile, plasticizers, biofuels, cosmetics, toiletries, food additives, candles and waxes, etc. [1]. The structure of oleochemicals having long-chain and double bonds facilitates the functionalization to produce a wide range of products. For example, linear alpha olefins (LAOs) from fatty acids of plant oil are one of the important key products to support the green and sustainable development in petrochemical manufacture. Since the LAOs are important commodity chemicals for using as petrochemical intermediates, the long-chain α-olefins are primarily used to manufacture everyday products such as plastic packaging (C_4-C_8), surfactants and detergents (C_{10}-C_{14}), and lubricant oil additives (C_{16}-C_{18}) for mechanics' engines [2, 3]. However, the current leading technology for long-chain α-olefins production is steam cracking (SC) during petroleum, natural gas refining or oligomerization of ethylene. The increase of olefin products has led to declining crude oil reserves and enhanced the chance of severe environmental problems including global warming. Therefore, investments in alternative processes and feedstocks have become an attractive route to promote the overall sustainability of the direct synthesis of olefins from renewable feedstocks.

Over decades, the production of olefins from fatty acids has been investigated under several chemical reactions such as deoxygenation, ethenolysis, and olefins' metathesis [4-6]. Deoxygenation is one of the famous reactions to transform fatty acids under an inert atmosphere. This reaction involves decarboxylation (DCO_2) or decarbonylation (DCO), which is endothermic process that needs high energy to remove -COOH and C=O bonds from molecules of fatty acids to generate hydrocarbons (HCs) with one less carbon atom than their inherent structures. Although the homogeneous catalysts consisted of transition metals based organometallic catalysts such as palladium (Pd), rhodium (Rh), iridium (Ir), ruthenium (Ru), nickel (Ni) and iron (Fe) show the high selectivity for LAOs synthesis (> 90%), the deoxygenation of fatty acids over heterogeneous catalysts has never achieved α-olefin products greater than 30% selectivity. Moreover, the formation of hydrogen gas (H_2) during deoxygenation leads the rapid hydrogenation of any alkenes formed resulting in the reduction of olefin selectivity and paraffins are produced as the dominant product [4].

To improve the performance and selectivity to long-chain α-olefins using heterogeneous catalysts, oxidative dehydrogenation (ODH) in an oxygen (O_2) atmosphere is attractive due to its many advantages, such as its exothermic nature resulting the milder operation, low carbon deposition, and lower costs than non-oxygen atmosphere reactions [7]. Moreover, ODH can inhibit alkane production from hydrogenation by consuming hydrogen and generating water as a by-product. Although ODH has already proved to be a good reaction for producing olefins from short-chain alkanes (C_2-C_4) and medium-chain alkanes (C_6-C_{12}) to olefins [8-13], there have been few reports focusing in the conversion of fatty acids for producing long-chain α-olefins via ODH reaction [14, 15].

Many kinds of catalysts have been tested for the ODH reaction, but transition metal-based oxides are the major group of catalyst applied for ODH of alkanes. Vanadium oxides supported on mesoporous silica, such as MCM-41, MCM-48, and

SBA-15, have been reported as an effective catalyst for ODH of light alkanes to produce olefins. The catalytic performance in the ODH of alkanes depends on the nature of the support, the vanadium loading, and the preparation conditions. These factors affect the nature and structure of the VO_x surface species [12, 16, 17]. Monomeric or low oligomeric V_xO_y species with V in octahedral and tetrahedral forms are active for reaction [12]. Although the tetrahedral vanadium species are less active than the octahedral ones, the vanadium in octahedral form has more selective; especially if it has a vanadium valence close to +4 [17]. On the other hand, the presence of polymeric and bulk V_2O_5 inhibited the activity of the catalyst as well as the formation of V_2O_5 crystallites toward deep oxidation [12, 17]. In addition, the basic oxides do not strongly adsorb the olefin products. This is different from the acidic oxides that have more ability to strongly adsorb olefins and promote oxidation to obtain carbon oxides (CO_x) [12, 18]. The use of mesoporous materials not only increases the surface area of the catalytic sites, but they also provide the higher dispersion of metal oxides and enhance the number of synergistic active sites [19]. Mesoporous materials, especially SBA-15, is one of the most extensively studied materials due to their impressive qualities such as high surface area, thick framework walls; which provide high hydrothermal stability, invariable cylindrical pores with large pore diameter; allowing easy diffusion of substrate molecules, enhanced their ability to anchor diverse chemical functionalities on their surface. Moreover, SBA-15 has shown excellent activity and selectivity in the catalytic oxidation of various hydrocarbons and alcohols to aldehydes, ketones, epoxides and acids [20]. Unlike MCM family, the poor hydrothermal/thermal stability is the major drawback of MCM support for the reactions operated under high-temperature and pressure. To consider the silica-based supports SBA-15 (two-dimensional) and KIT-6 (three-dimensional), the unique 3D-mesoporous feature of the KIT-6 material is expected to maximize the diffusion ability of reactant molecules into the channels without blocking any pores than SBA-15 [19, 21, 22]. Whereas, the synthesis method of SBA-15 is not complicated and takes a shorter time than as the KIT-6 synthesis method [23, 24].

According to the advantage of ODH in the olefin production as described above, this research aimed to study the possibility to transform oleic acid (OA), which is the abundant fatty acid component in palm oil, to produce long-chain α-olefins via ODH using V_xO_y/SBA-15 catalyst. The catalyst performance was investigated through the factors of vanadium content and reaction temperature on OA conversion, long-chain olefin selectivity, and chemical compositions in the obtained liquid product. Moreover, the catalyst stability and its reusability over four consecutive cycles were reported.

1.2 Research objectives

1.2.1 To study the production of bio-olefins from ODH of OA using vanadium oxides supported on SBA-15 catalysts (V_xO_y/SBA-15).

1.2.2 To study the effects of reaction parameters such as vanadium content (wt%) based on SBA-15, reaction temperature, catalyst stability, and reusability of catalyst on the selectivity to bio-olefins obtained from the ODH of OA.

1.2.3 To monitor the durability and reusability of the V_xO_y/SBA-15 catalyst.

1.3 Research scopes

1.3.1 To prepare and characterize the V_xO_y/SBA-15 catalysts before and after ODH of OA.

1.3.2 To investigate the effects of reaction parameters on the OA conversion and the selectivity to olefins in the liquid and gaseous products.

1.4 Research methodology

1.4.1 Study the previous literatures, provide chemicals used in this research and set up the fixed bed reactor for ODH process.

1.4.2 Prepare SBA-15 via hydrothermal method and V_xO_y/SBA-15 catalyst by wet impregnation method.

1.4.3 Characterize catalysts with several techniques:

1.4.3.1 X-ray diffraction (XRD)

1.4.3.2 Surface and pore size analysis (Nitrogen physisorption)

1.4.3.3 Ammonia temperature programed desorption (NH_3-TPD)

1.4.3.4 Hydrogen temperature programed reduction (H_2-TPR)

1.4.3.5 X-ray photoelectron spectra (XPS)

1.4.3.6 Transmission electron microscopy with an energy dispersive X-ray (TEM-EDX)

1.4.3.7 Scanning electron microscopy (SEM)

1.4.4 Study the effect of reaction parameters on ODH of OA. The OA conversion, product selectivity, and product yields for both liquid and gaseous products were monitored.

1.4.4.1 Vanadium content on SBA-15: 0.5, 1.0, 3.0, and 5.0 wt%

1.4.4.2 Reaction temperature: 400 – 550 $^{\circ}$C

1.4.4.3 Time on stream: 2, 6, and 8 h

1.4.4.4 Regenerated and reusability: 4 cycles

1.4.5 Analyze the products obtained from ODH of OA over V_xO_y/SBA-15 catalysts

1.4.5.1 Liquid product: chromatograph-mass spectrometer (GC-MS) to identify types and their relative contents of components in the liquid product.

1.4.5.2 Gas product: chromatograph-flame ionization detector (GC-FID) for analyzing the amount of light hydrocarbon (C_{1-5}) and gas chromatograph-thermal conductivity detector (GC-TCD) to determine the amounts of H_2, CO and CO_2 content.

1.4.5.3 Solid product: thermogravimetric analysis (TGA) was used to quantify the amount of coke deposited on the catalyst's surface.

1.4.6 Discuss the obtained results and thesis writing.

1.5 Expected benefits

To achieve the appropriate conditions for maximizing the levels of OA conversion and selectivity to bio-olefins from ODH process over V_xO_y/SBA-15 catalysts.

จุฬาลงกรณ์มหาวิทยาลัย
CHULALONGKORN UNIVERSITY

CHAPTER II

THEORY AND LITERATURE REVIEWS

2.1 Olefins

Olefins or alkenes are a class of unsaturated hydrocarbons with at least one carbon-to-carbon double bond (C=C) or triple bond. Ethylene (C_2H_4), propylene (C_3H_6), 1,3-butadiene (C_4H_6) are example of olefins, which are important commodity chemicals and petrochemical intermediate. Application of olefins is depended on a number of carbon atoms in their molecules and the position of C=C bonds in their chain, especially the C=C bond at terminal position of hydrocarbon chain or called as alpha-olefins (α-olefins) because they can participate in various reactions such as prominently polymerization and alkylation.

2.1.1 Short-chain olefins or light olefins (C_2-C_4)

Olefins with a chain length consisted of 2-4 carbon atoms are the most important building blocks of the chemical industry. They are currently mostly manufactured using steam cracking, fluid catalytic cracking, and on-purpose synthesis techniques such as ethane and propane dehydrogenation. [25].

2.1.1.1 Ethylene (C_2H_4)

As shown in Figure 2.1, ethylene is widely used in the chemical industry, where the most of the production goes toward polyethylene (PE) such as HDPE, LDPE, or LLDPE that mainly utilized in the production of plastics [26]. Other compounds such as vinyl chloride (generate PVC), ethene oxide (contain in pesticide and a sterilizing agent), and ethylbenzene (precursor to polystyrene) are also produced from ethylene.
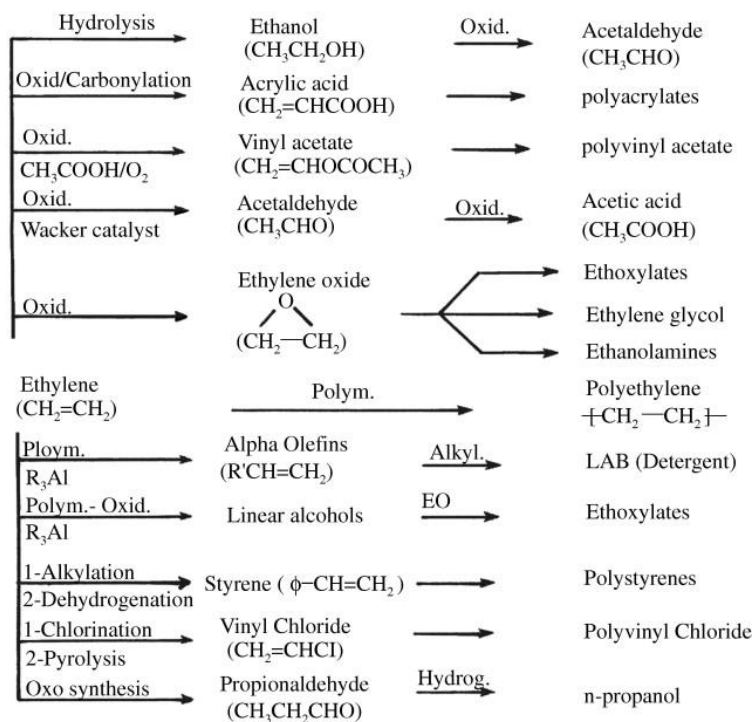
Figure 2.1 Major chemicals derived from ethylene [27].

2.1.1.2 Propylene (C_3H_6)

Propylene is a building-block chemical base, which is mostly used in the manufacture of polymers such as polypropylene (PP), polyurethane (PU) and epoxy resins along with other materials. The chemicals produced from propylene include, polypropylene (plastic resin, plastic squeeze bottles, outdoor furniture) acrylonitrile (used to make acrylic fiber and coatings), propylene oxide (towards to polyurethane), cumene (make phenol and acetone), and isopropyl alcohol (make solvents, cosmetics, household cleaners and pharmaceuticals), as shown in Figure 2.2 [28].
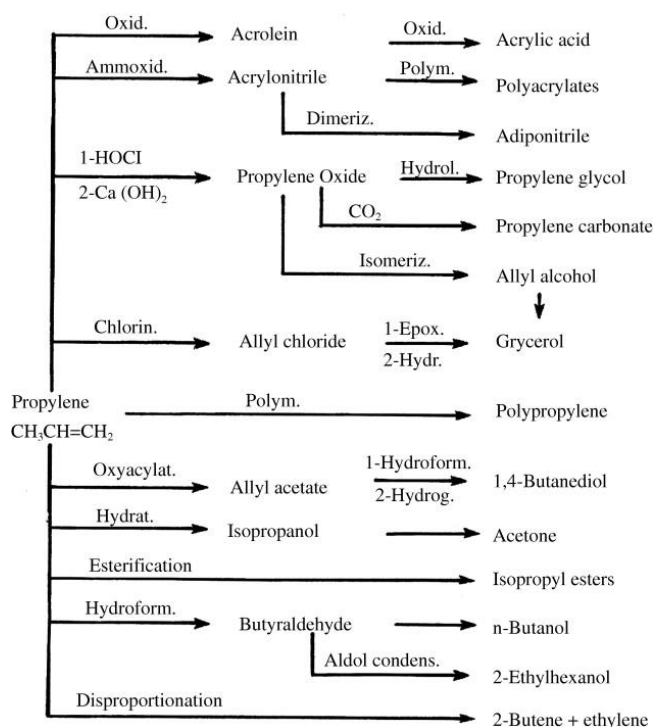
Figure 2.2 Major chemicals derived from propylene [27].

2.1.1.3 Butadiene (C_4H_6)

The main applications of butadiene are synthetic rubber, such as butadiene rubber (BR), nitrile-butadiene rubber (NBR), and neoprene. Moreover, butadiene combined with styrene are used to produce various kinds of resins, such as ABS (acrylonitrile-butadiene-styrene) resin, SBS (styrene-butadiene-styrene triblock) resin, and BS (butadiene-styrene) resin. These are widely used in producing shoe soles, tyres and other parts for the car industry, adhesives and sealants, asphalt and polymer modification [29].

2.1.2 Long-chain olefins ($\geq C_{10}$)

The long-chain olefins currently synthesized via the direct ethylene oligomerization or thermal cracking of long-chain paraffins. They are mostly in a form of linear-alpha olefins (LAOs), which are primarily used to manufacture everyday products

such as surfactants and detergents (C_{10}-C_{14}), lubricant oil additives (C_{16}-C_{18}) for mechanics' engines, and synthesis of wax (C_{20+}) [30].

2.2 Olefins production

2.2.1 Steam cracking (SC) [27]

The SC of hydrocarbons is one of the most important and energy-intensive processes in the petrochemical industry for producing light olefins, especially ethylene and propylene. This process is a thermal cracking process without a catalyst, which is performed in the presence of steam at high temperatures and short residence times. During the steam-cracking operation, steam acts as a diluent to suppress the hydrocarbon partial pressure for decreasing the formation of coke deposition by gasification reaction. The hydrocarbons primarily originated from crude oil are cracked in the tubular reactors suspended in a gas-fired furnace. Steam-cracking produces a variety of products. Not only produce light olefins, but it also generated a group of C_4 hydrocarbons containing paraffins, olefins, and butadiene.

2.2.2 Fischer-Tropsch (FT) synthesis [31]

The FT synthesis is another technology to convert syngas (CO+H_2) as the hydrocarbons by the assistance of catalysts. The generated products are consisted of linear paraffins, α-olefins, and small amount of oxygenated compounds (alcohols, ketones, aldehydes) as shown in Table 2.1. The selectivity in the FT synthesis is depended on various parameters, and the determination of the selectivity is complicate. For example, the operation of the reaction is carried out at a high temperature (340°C) and usually provides the short-chain hydrocarbons. Whereas, the lower temperature (230°C) mostly produces the long-chain hydrocarbons.

Although ruthenium (Ru), nickel (Ni), cobalt (Co), and iron (Fe) metals exhibit catalytic activity for the FT process, Ru is unsuitable for commercial applications

when metals' market prices are taken into account. Whereas, Ni metal provides a very high methane selectivity. For this reason, the Co or Fe is preferred in all FT process. The Co catalyst is applied in low temperature since it increases methane formation at high temperatures. The product formed by Co catalyst is usually consisted of linear hydrocarbons. Whereas, the Fe catalyst can be used at both low and high reaction temperature in the FT process. The main product obtained when the system is operated at high temperatures consists mainly of alkene products, while operating at low temperatures provides the mixture containing alkane products.

Table 2.1 Fischer–Tropsch synthesis reactions [32].

Main reactions	
1. Methane	$CO + 3H_2 \rightarrow CH_4 + H_2O$
2. Paraffins	$(2n + 1)H_2 + nCO \rightarrow$ $C_nH_{2n+2} + nH_2O$
3. Olefins	$2nH_2 + nCO \rightarrow C_nH_{2n} + nH_2O$
4. Water gas shift (WGS) reaction	$CO + H_2O \rightarrow CO_2 + H_2$
Side reactions	
5. Alcohols	$2nH_2 + nCO \rightarrow C_nH_{2n+1}O + nH_2O$
6. Boudouard reaction	$2CO \rightarrow C + CO_2$
Catalyst modifications	
7. Catalyst oxidation/ reduction	a. $M_xO_y + yH_2 \rightarrow yH_2O + xM$
	b. $M_xO_y + yCO \rightarrow yCO_2 + xM$
8. Bulk carbide formation	$yC + xM \rightarrow M_xC_y$

2.2.3 Oligomerization of ethylene

Oligomerization of ethylene is the basic-reactions to produce the linear-alpha olefins (LAOs) containing the number of carbons ranging from C_4 to C_{20+}, as shown in Figure 2.3. In the polymerization of small olefins such as ethylene and propylene, both heterogeneous and homogeneous catalytic systems are operational. For heterogeneous catalyst, Ziegler–Natta catalyst supported based on titanium compounds with the combination of co-catalysts (e.g., organoaluminum compounds such as triethylaluminium ($Al(C_2H_5)_3$)) is used in polymerization. Whereas, a large

number of specialty polyolefins have been produced with homogeneous metallocene catalysts, usually based on complexes of the group 4 metals such as titanium (Ti), zirconium (Zr) or hafnium (Hf) dissolved in the organic solvent [33].
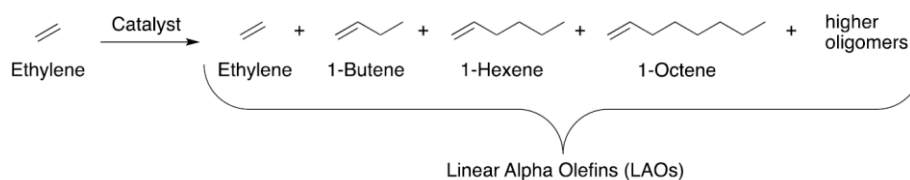
Figure 2.3 LAOs synthesis via the oligomerization of ethylene [34].

2.3 Alternative process of olefins

2.3.1 Oxidative dehydrogenation of alkanes [28]

The oxidative dehydrogenation (ODH) of alkanes is a promising alternative way for the production of short-chain olefins (C_2-C_4) and some long-chain olefins (C_6 and C_8). There are no thermodynamic limitation, and accordingly olefins can be produced at lower temperature than steam cracking process since ODH is an exothermic process that does not require a heat supply. Moreover, the presence of oxygen in the system can be helpful for inhibiting the coke formation. To compare the heat of reaction generated by the direct dehydrogenation as shown in Eq.(2.1), the ODH in Eq.(2.2) shows the lower enthalpy for producing olefins.

$$C_2H_6 \rightarrow C_2H_4 + H_2 \qquad \Delta H^0_{298} = +136 \, kJ \, mol^{-1} \qquad (2.1)$$

$$C_2H_6 + \frac{1}{2}O_2 \rightarrow C_2H_4 + H_2O \qquad \Delta H^0_{298} = -105 \, kJ \, mol^{-1} \qquad (2.2)$$

Among the supported catalysts applied for ODH process, vanadium and molybdenum have already proved to be the most active and selective. The vanadium based catalyst has higher activity to catalyze ODH than molybdenum at equivalent metal dispersion [12]. Vanadium oxides supported on mesoporous silica, such as MCM-41, MCM-48, and SBA-15, have been reported as an effective catalytic system for ODH of light alkanes to produce olefins [12, 16, 17]. Due to the basic supports, the higher

vanadium dispersion yielded the better ODH performance [12, 18]. Monomeric or low oligomeric V_xO_y species with V in octahedral and tetrahedral form are the active for the reaction. Although the tetrahedral vanadium is less active than the vanadium in octahedral form, the vanadium in the tetrahedral form had the higher selectivity, especially if it has a vanadium valence close to +4. On the other hand, the presence of polymeric and bulk V_2O_5 inhibits the activity of the catalysts as well as the formation of V_2O_5 crystallites for promoting the deep oxidation. In addition, another advantage of the use of basic oxides as the catalyst's support is the lower ability to promote the strong adsorption of olefins during the reaction. These acidic oxides have higher performance to induce the adsorption of olefins and promote oxidation to obtain carbon oxides (CO_x).

2.4 Oleochemicals from palm oil

2.4.1 Palm oil

Palm oil derived from the oil palm fresh fruit bunch (FFB), which contains 20%-25% oil, and the rest is moisture and biomass. There are two different types of oil that can be extracted from the palm fruit (Figure 2.4): crude palm oil (CPO) and crude palm kernel oil (CPKO) from the fibrous mesocarp and kernels, respectively. Although both oils originate from the same fruit, palm oil is chemically and nutritionally different from palm kernel oil, as shown in Table 2.2. The major fatty acids of palm oil are palmitic acid (C18:0) and oleic acid (C18:1), whereas palm kernel oil mainly contains lauric acid (C12:0) and myristic acid (C14:0). The high-quality palm oil used in the edible oil industry contains a large number of neutral triacylglycerols (TAGs) (Figure 2.5) (95%) and low free fatty acids (less than 0.5%), low impurity content, and good bleaching. Furthermore, the transformation of fatty acids found in palm oil through the oleochemical industry is alternative to enhance the product's value and its sustainability with environmental friendly nature.
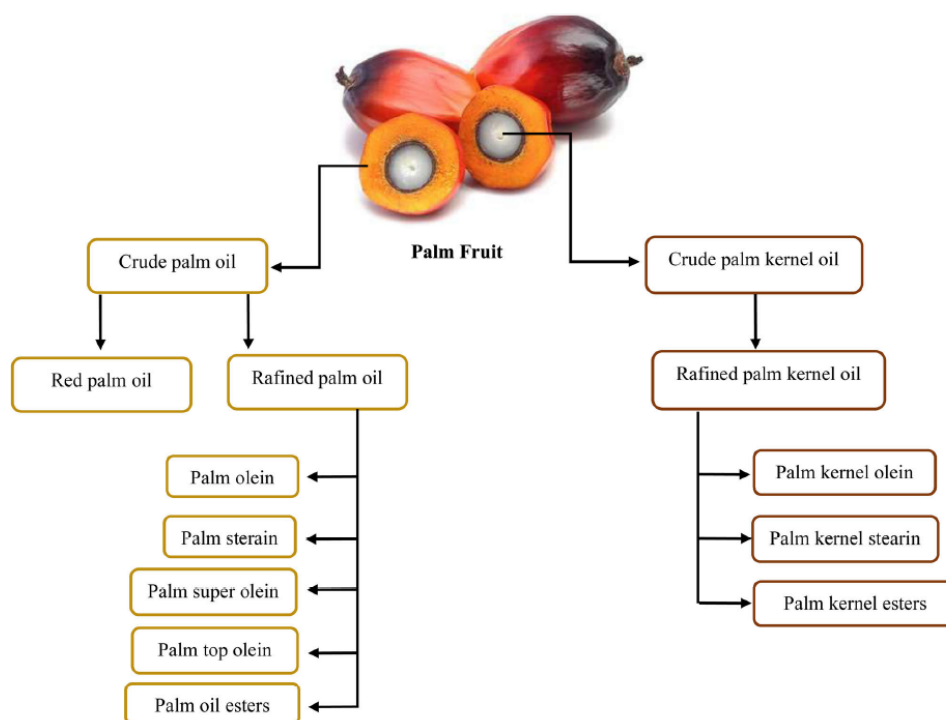
Figure 2.4 Fractional oil types obtained from palm fruit [35].

Table 2.2 Fatty acids in palm oil, palm kernel oil, and palm oil's derivates [35]

Type of oil	Main fatty acids	SFAs (g/100 g)	MUFAs (g/100 g)	PUFAs (g/100 g)			Reference
				Total	n-6	n-3	
Palm oil	Palmitic acid Oleic acid Linoleic acid	47.8	37.1	10.4	10.1	0.3	(Foster, Williamson, and Lunn 2009)
Palm kernel oil	Lauric acid Myristic acid Oleic acid	81.5	11.4	1.6	1.6	0	(USDA 2020)
Palm olein	Palmitic acid Oleic acid Linoleic acid	45	42	11	11	0	(Campbell et al. 2006)
Palm super olein	Oleic acid Palmitic acid Linoleic acid	36.5	46.3	13.6	13	0.6	(T.C. Tarım ve Orman Bakanlığı 2015)
Palm stearin	Palmitic acid Oleic acid	68	26	7	6.5	0.5	(T.C. Tarım ve Orman Bakanlığı 2015)

SFA: saturated fatty acid, MUFA: Monounsaturated fatty acid, PUFA: Polyunsaturated fatty acid
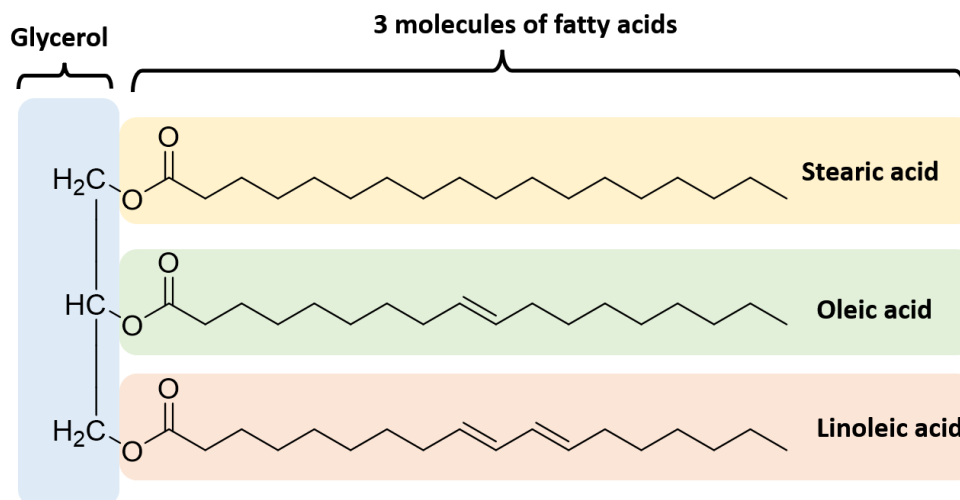
Figure 2.5 General structure of triglycerides in palm oil.

2.4.1 Oleochemicals

Oleochemicals are chemical components derived from sustainable resources that are mainly oils and fats of vegetable and animal sources, such as coconut oil, palm oil, palm kernel oil, soybean oil, sunflower seed oil, and animal fat. The natural oleochemicals are firstly produced from the triglycerides-based in vegetable oils via hydrolysis or transesterification to further obtain three fatty acids and one molecule of glycerin [1]. These fatty acids are almost entirely straight long-chain carboxylic acids (C_4-C_{22}). The fatty acid containing C_{18} are mostly in the forms of stearic acid (saturated structure), oleic acid (mono-unsaturated structure), and linoleic acid (poly-unsaturated structure). These fatty acids have potential to be converted as the long-chain olefins, which can substitute the petroleum feedstock used in many applications such as pharmaceuticals, plasticizers, rubber, adhesive, glue, greases and lubricants, biofuels, paints, coatings, detergents, surfactants, cosmetics, soap, candles and waxes, and others [1].

Among many kinds of vegetable oils, palm oil presents the best choice over other oil crops for use in the oleochemical industry due to its high productivity and competitive price. Moreover, it is abundant and a lot of manufacturers can be found in

South East Asia (SEA). Palm oil is significantly cheaper than soybean oil and the most affordable oil for consumers in low-income countries. In addition, oil palm can be grown on ground that would otherwise be unsuitable for other crops and require less fertilizer, pesticides and energy. These reasons promote palm oil is one of high eco-friendly choices. Since, palm oil availability on the market has largely increased over the last 20 years resulting from the booming palm oil production, palm oil is attractive and suitable for using as a renewable feedstock in the oleochemical industry [36-38].

2.5 Heterogeneous catalysts used in oxidative dehydrogenation (ODH)

2.5.1 Heterogeneous catalysts

Heterogeneous catalysts are easy to separate from reaction production and have higher thermal stability than homogeneous catalysts. Among various kinds of catalysts, the transition metal-based oxides are the major group of catalysts applied for ODH. Vanadium (V) and molybdenum (Mo) have been found to be the most active and selective catalysts for the ODH of light alkanes [12]. However, vanadium has higher ODH activity than molybdenum at equivalent dispersion. The catalytic performance in the ODH depends on the nature of the support, the vanadium loading, and the preparation conditions. These factors affect the nature and structure of the V_xO_y surface species. Vanadium oxides supported on mesoporous silica materials not only increases the surface area of the catalytic sites, but they also provide the higher dispersion of metal oxides and enhance the number of synergistic active sites [19].
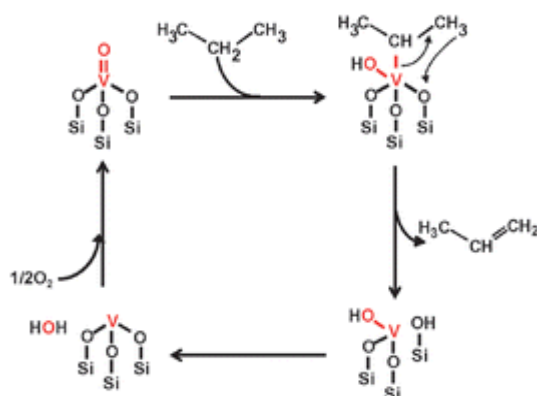
Figure 2.6 Mechanisms of oxidative dehydrogenation over VO$_x$/SBA-15 catalyst [39].

2.5.2 Mesoporous silica-supported

In 1998, Stucky and his group synthesized another type of hexagonal array of pores called Santa Barbara Amorphous (SBA), especially SBA-15, which has attracted the interest of many researchers due to its remarkable features such as high surface area, large pore size (5–30 nm), the well-defined pore structure with uniform cylindrical pores, thick pore wall, high thermal and hydrothermal stability that make them suitable for various applications in catalysis, drug delivery, immobilization, and chromatographic techniques [19]. The synthesis of SBA-15 involves hydrolysis and condensation of the silica source. The dissolving of the template (nonionic triblock copolymer, Pluronic P123) in an acidic solution, followed by the addition of the silica source (tetraethoxysilane, TEOS). The mixed solution was heated at 30–40 $^\circ$C for 20–24 h and then aged for 24–48 h at 80–120 $^\circ$C. After aging, the obtained solid was filtered and washed many times with DI water. The sample is first air dried overnight at room temperature before being dried in an oven at 80 $^\circ$C for 5–6 h. Finally, the sample is calcined at 550 $^\circ$C for 4–6 h for template removal.

Currently, SBA-15 mesoporous material has been investigated as potential support in the field of catalysis due to its intrinsic structural features like a thick framework wall providing high hydrothermal stability and a large pore diameter allowing

easy diffusion of substrate molecules. Moreover, SBA-15 has shown excellent activity and selectivity in the catalytic oxidation of various hydrocarbons and alcohols to aldehydes, ketones, epoxides, and acids, as shown in Table 2.3.

Table 2.3 Applications of SBA-15 support in some catalytic oxidation reactions [19]

SBA-15 supported catalyst	Application	Oxidant	Reaction conditions	Remarks
Fe/SBA-15	Oxidation of styrene	H_2O_2	P = atmospheric T = 50–70 °C	Catalyst was prepared by new and simple method of physical vapour infiltration and benzaldehyde was found as the main reaction product (>90%)
Co/Ce-SBA-15	Oxidation of benzene	O_2	P = atmospheric Temp = 200–340 °C Flow rate: 320 ml/min	Ce-SBA-15 support was first time reported for deep oxidation of benzene and showed high catalytic activity for oxidation of benzene
Pt/SBA-15, Pd/SBA-15	Oxidation of toluene	O_2	P = atmospheric T = 25–300 °C Flow rate: 100 ml/min	SBA-15 support was prepared by direct and post synthesis technique. 0.5 wt% Pd/SBA-15 and 1.0 wt% Pt/SBA-15 catalysts were found to be most active
Pd/TiO$_2$-SBA-15	Oxidation of methane	O_2	P = atmospheric Temp = 200–600 °C Flow rate: 50 ml/min	10 wt% of TiO$_2$ loading over Pd/SBA-15 increased the catalyst activity and sulphur tolerance in comparison to Pd/SBA-15

SBA-15 supported catalyst	Application	Oxidant	Reaction conditions	Remarks
Au/CeO$_2$-SBA-15	Oxidation of carbon mono oxide	O$_2$	P = atmospheric Temp = 30–500 °C	Au catalyst supported over SBA-15 with different CeO$_2$ loadings (5–30 wt%) were prepared and optimum performance was found for 20 wt% ceria loading
Cu/SBA-15	Oxidation of alkyl aromatics	TBHP	P = atmospheric Temp = 27–100 °C	10 wt% of Cu loading over SBA-15 support was found to be efficient for the benzyl oxidation of alkyl aromatics
Pd/Al-SBA-15	Oxidation of cinnamyl alcohol	O$_2$	P = atmospheric Temp = 90 °C	Conversion was ≥95% during the first hour and ≥90% after 24 h
Re/SBA-15	Oxidation of n-alkanes	O$_2$	Pressure 15 bar Temp = 80–200 °C	For C$_5$-alkane overall conversion was 19.6 and 22.6% for C$_6$-alkane
Ag/Al-SBA-15	Oxidation of carbon monoxide	O$_2$	P = atmospheric Temp = 20–140 °C Flow rate: 30 ml/min	Catalysts were prepared by in situ 'pH adjusting' method and the effect of Si/Al ratio on the structure of Ag catalyst and catalytic activity was investigated
Cu/CuO/SBA-15	Oxidation of benzyl alcohol	H$_2$O$_2$	P = atmospheric Temp = 80 °C	73% conversion of benzyl alcohol and 54% selectivity of benzaldehyde was achieved by chemical reduction synthesis method

2.6 Literature reviews

Mitran et al. [12] studied the catalytic activity of VO_x/SBA-15 having vanadium loading at 6.5-11 wt%. This catalyst was prepared by wet impregnation method and its catalytic performance on ODH of propane at 450-600 ^{O}C was observed. The results from catalyst characterization exhibited the well-dispersion of vanadium (monomeric and oligomeric, VO_4^{3-}) on SBA-15 at low vanadium content (6.5 wt%), while the increasing vanadium content to 11.0 wt% obviously presence the vanadium agglomeration (V_2O_5 crystalline). Although the higher vanadium loading induced the higher activity, the selectivity to propene was lower, as shown in Table 2.4. The result of catalytic performance showed that the low vanadium content (6.5 wt%) exhibited the highest selectivity to propene (87% selectivity) and gradually decreased to 38% selectivity when the vanadium content increased to 11 wt%. However, the increases in the vanadium content showed the highest performance to achieve 21% propane conversion when ODH was operated at 600 ^{o}C. Although the higher reaction temperature could improve the catalyst performance, it enhances the change of cracking and further oxidation to obtain CO_x.

Table 2.4 Propane conversion and product selectivity values in the ODH of propane [12]

Catalyst sample	Temperature (°C)	Propane conversion (%)	Selectivities (%)			E_{act}^{a} (kJ mol^{-1})
			Propene	Cracking	CO_x	
6.5V	450	0.5	87	1	12	158
	500	2.8	80	2	18	
	550	12.1	68	3	29	
	600	16.3	66	5	29	
7.5V	450	0.6	84	1	15	152
	500	3.9	74	1	25	
	550	12.9	64	2	34	
	600	17.5	62	3	35	
9V	450	0.8	83	1	16	141
	500	5.1	72	2	26	
	550	13.7	59	5	36	
	600	18.5	57	7	36	
10V	450	1.1	73	1	26	130
	500	6.0	65	1	34	
	550	14.9	44	2	54	
	600	19.6	41	5	54	
11V	450	1.5	71	1	28	119
	500	6.8	58	1	41	
	550	16.3	39	2	59	
	600	21.6	38	4	58	

^{a} Apparent activation energy.

Elkhalifa et al. [9] studied the ODH of n-octane using VMgO catalysts with different vanadium loadings (5 ,15, 25, 50 wt%) in a continuous flow fixed bed reactor at GHSV of 6,000 h^{-1} and 350–550 $^\circ$C using air as an oxidant and nitrogen as a make-up gas to give 9% n-octane in the gaseous mixture. The results showed that all catalysts achieved high performance to convert n-octane when the temperature increased. The product selectivity to octene was depended on vanadium content, as shown in Figure 2.7. The 50-VMgO catalyst exhibited the highest selectivity to octenes, which 3-octene was the dominant isomer and 1-octene was rarely observed. Whereas, the dominant product obtained from ODH catalyzed by 15-VMgO catalyst was 1-octene. Moreover, cyclization of C_1 to C_6 was predominantly occurred and led to the formation of styrene and ethylbenzene over xylene.
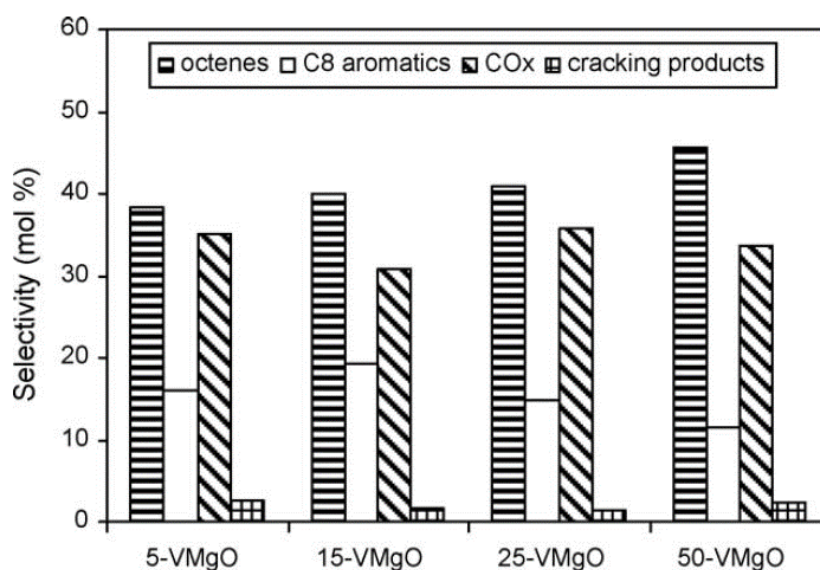
Figure 2.7 Products selectivity on different catalysts at 450 $^\circ$C and isoconversion [9]

Sancheti et al. [40] studied a new catalyst NiMoK/TS-1 for decarboxylation of methyl palmitate. The effect of support's acidity and molybdenum loading on the methyl palmitate conversion along with the product selectivity into C_{15} olefin was investigated. The reaction was carried out using a vapor-phase fixed-bed downflow reactor system at atmospheric pressure. The results of olefins selectivity shown in Table 2.5 indicated that Ni_5Mo_{10}-K/TS-1 catalyst exhibited the highest selectivity to C_{15} olefin, whereas the higher acidity of catalyst promoted the higher performance to achieve 57% methyl palmitate conversion. The Ni_5Mo_{10}-K/TS-1catalyst at a weight hourly space velocity (WHSV) of 5.6 h^{-1} was also selective toward C_{15} olefin. When the reaction was performed at $380^{\circ}C$ reaction temperature, the conversion of methyl palmitate increased whereas the selectivity to C_{15} products and C_{15} olefin decreased. Moreover, the catalyst performance dramatic decreased when the long time on stream (over 15 h) was applied. The Ni_5Mo_{10}-K/TS-1catalyst showed the high efficiency for reusable. It can be regenerated with no considerable decrease in the activity even after fourth reuse.

Table 2.5 Effect of different catalysts on the conversion of methyl palmitate and selectivity of C_{15} products [40]

catalyst	Mo-K/Al	Ni_5Mo_5/TS (1:10)	Ni_5Mo_5/TS-1	Ni_5Mo_{10}/TS-1	Ni_5Mo_{10}-K/TS-1
acidity (mmol/g)	1.24	0.487	0.15	0.202	0.176
conversion (%)	57 ± 2	44 ± 2	41.3 ± 2	38.7 ± 1	28.2 ± 1
selectivity for C_{15} (%)	39.8 ± 2	63.4 ± 3	88.3 ± 3	92 ± 2	95 ± 2
C_{15} paraffin/C_{15} (%)	81.1	59.8	23.3	11.7	9.4
C_{15} olefin/C_{15} (%)	18.9	40.2	76.7	89.3	91.7
selectivity of C_{15} olefin (%)	7.5	25.5	67.73	82.16	87.1
C_n, $n < 15$	54.6	33.4	10.4	7	3.4
C_{16} hydrocarbons (%)	1.6	0.5	0.2	0.1	0.1
C_{16}, C_{17} oxygenates (%)	4.1	3.3	1.4	1	0.6

Krobkrong et al. [41] studies the deoxygenation of oleic acid under N_2 atmosphere over molybdenum oxide catalysts with promoters (Ni, Co, and Cu) and varying catalyst loadings (19–34 wt%) on γ-Al_2O_3 support. All catalyst prepared by an incipient wetness impregnation method. The obtained green diesel hydrocarbon is the main desired product. The catalytic testing was carried out in a batch reactor for 3–9 h at temperatures 300–350 °C under N_2 pressure (10 and 40 bar). Figure 2.8 showed the conversion and liquid products distribution via deoxygenation of oleic acid. The 19 wt% of NiMo oxide on γ-Al_2O_3 exhibited the highest performance for oleic acid conversion (81% conversion), and increased the amount of targeted C_{17} hydrocarbons. However, stearic acid and saturated hydrocarbons are also found during the deoxygenation of oleic acid under N_2 atmosphere. These implied that the competition between dehydrogenation and hydrogenation reaction could occur when using metal oxide catalysts. The longer reaction time and higher temperature enhances the conversion of oleic acid toward 96%, whereas the selectivity to the desired C_{17} products was only 57% when the reaction was operated at 330 °C 24 h. For catalyst reusability, the NiMo oxide catalyst demonstrated the high efficiency of reusable. It could be regenerated with no considerable decrease in the activity even after fourth reuse.
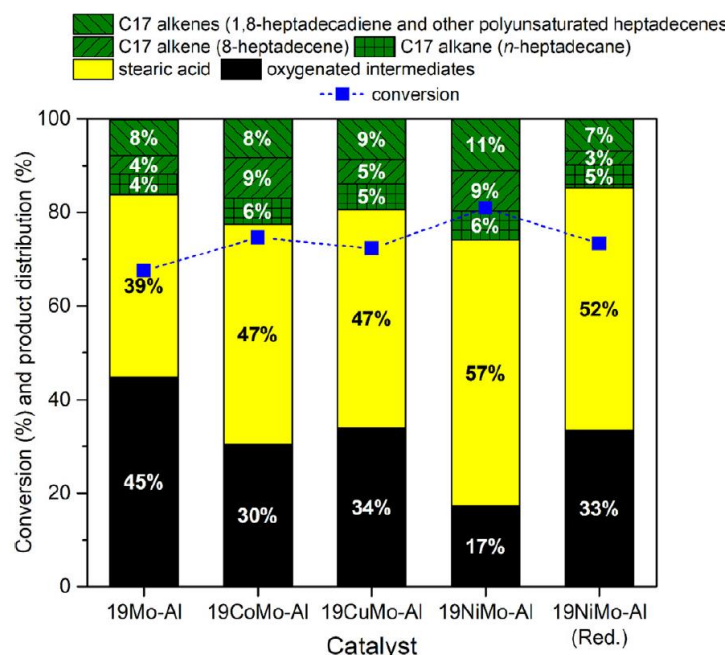
Figure 2.8 Conversion and liquid product distribution obtained by deoxygenation of oleic acid using MoO_3-based catalysts under 40 bar initial N_2 pressure at 330 °C for 3 h [41].

Chatterjee et al. [42] studied, the transformation of fatty acids to α-olefins using commercial Pd/C, in combination with phosphine ligands to promote decarbonylative dehydration. The results showed that the combination of a heterogeneous Pd/C catalyst in the presence of phosphine ligands with free-solvent provided the 20-fold higher activity (TOF = 420 h^{-1}) and the selectivity to α-olefins increased to > 95% at the optimized conditions. The long-chain fatty acids (C_{10}-C_{18}) were converted to the olefins in the good yield with high α-selectivity. Moreover, the catalyst could easily be recycled at least twice without loss of activity or selectivity.

CHAPTER III

EXPERIMENTAL

This chapter shows chemicals, materials, experimental procedures for preparation of the catalysts and oxidative dehydrogenation (ODH) of oleic acid (OA) to generate the long-chain bio-olefins.

3.1 Reactant and chemicals

3.1.1 Tetraethyl orthosilicate (TEOS, 99% purity, Sigma Aldrich, USA)

3.1.2 Triblock copolymer Pluronic P123 ($EO_{20}PO_{70}EO_{20}$, Mw = 5,800, Sigma Aldrich, USA)

3.1.3 Ammonium vanadate solution (NH_4VO_3, > 99% purity, Sigma Aldrich, USA)

3.1.4 Oleic acid (OA, 90% purity, Sigma Aldrich, USA)

3.1.5 Oxygen gas (O_2, 99.99%, Bangkok Industry Gas, Thailand)

3.1.6 Nitrogen gas (N_2, 99.99%, Praxair, Thailand)

3.1.7 Standard gases (the mixed hydrocarbon C_1-C_4 gases, RIGAS Co.,Ltd., Korea)

3.1.8 Standards gases (the mixed gases containing H_2, CO, and CO_2, Linde (Thailand) Co.,Ltd., Thailand)

3.2 Apparatus

3.2.1 A fixed bed reactor (inside diameter = 9.525 mm; length = 14 cm) made from stainless steel was used for the ODH of OA. This unit was consisted of a heater and a temperature controller, mass flow controller, and HPLC pump for feeding the reactant as shown in Figure 3.1

3.2.2 Hot air oven (Binder, German)

3.2.3 Hot plate stirrer (IKA, C-MAG HS7)

3.2.4 Muffle furnace (Carbolite Gero, 30-3000 $^{\circ}$C)

3.2.5 Rotary evaporator (Heidolph, Hei-vap)
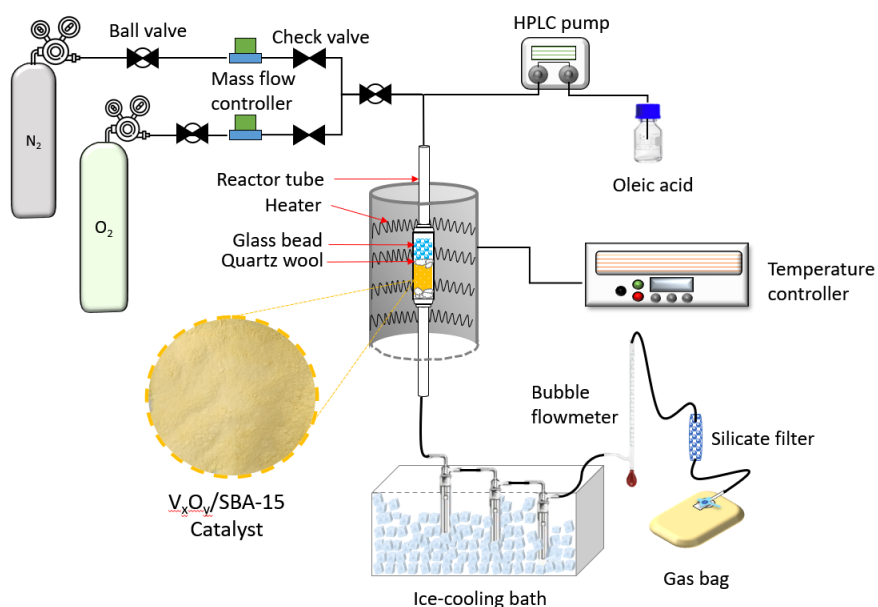
Figure 3.1 Schematic representation of the fixed-bed reactor used for ODH of OA.

3.3 Catalyst preparation

3.3.1 Preparation of SBA-15 support [24]

The SBA-15 support was prepared via hydrothermal method. Tetraethyl orthosilicate (TEOS) and the Pluronic P123 were used as a silica source and a structure directing agent, respectively. Pluronic P123 (3.8 g) was dissolved in the mixture containing 90 mL deionized (DI) water and 60 mL HCl solution (4 M) at 35 $^{\circ}$C for 2 h under stirring until the homogeneous solution was obtained. TEOS (8 g) was then added dropwise into the above solution under stirring at this temperature for 24 h. The resultant was then transferred into the Teflon autoclave for conducting the hydrothermal treatment performed at 80 $^{\circ}$C for 24 h without stirring. The solid product was collected by filtration, washed with DI water several times and dried at room temperature for 2 h before drying in an oven at 110 $^{\circ}$C for 12 h. The dry support was then calcined at 550 $^{\circ}$C for 6 h at a heating rate of 5 $^{\circ}$C min^{-1} to remove the organic template and condensed silanol groups.

3.3.2 Preparation of nV$_x$O$_y$/SBA-15 catalyst

The catalysts containing the different vanadium loadings (0.5, 1.0, 3.0 and 5.0 wt%) were prepared by wet impregnation. The calcined SBA-15 (1 g) was dispersed in 12 mL ammonium vanadate solution (NH$_4$VO$_3$) at desired concentrations under stirring at 60 ^{o}C for 2 h The obtained products were then dried by using a rotary evaporator at 60 ^{o}C and dried in the oven at 110 ^{o}C overnight before calcination at 600 ^{o}C for 5 h at a heating rate of 5 ^{o}C min^{-1}. The obtained calcined catalysts were labelled as nV$_x$O$_y$/SBA-15, where n was the vanadium loading (0.5–5.0 wt%).

3.4 Oxidative dehydrogenation (ODH) of oleic acid (OA)

The ODH of OA was carried out in a fixed bed reactor placed in a vertical tubular furnace. The system was operated in a down-flow mode. The 0.2 g catalyst was loaded between two layers of glass wool, while the free space above the glass wool was filled with 2 g glass beads to prolong the residence time for transforming OA as the vapor phase before passing through the catalyst bed, as shown in Figure 3.1. The reaction was performed in the presence of 1/1 (v/v) O$_2$/N$_2$ mixed gas at 1 atm with 2,600 h^{-1} gas hourly space velocity (GHSV). Typically, the reactor was heated to the desired temperature (400-550 ^{o}C) and then allowed to stabilize for 1 h before feeding the OA into the reactor by using an HPLC pump at a flow rate of 0.1 mL min^{-1}, which was equivalent to 26 h^{-1} weight hourly space velocity (WHSV). When the reaction was allowed for 2 h, the cumulative liquid product was collected by trapping the condensable vapor in an ice-cooling bath. Simultaneously, the gaseous product was also collected in a gas bag (10 L) during the reaction. All experiments were duplicated and the average values with standard deviation was reported.

3.5 Catalyst characterization

3.5.1 X-ray diffraction (XRD)

The X-ray diffraction (XRD) patterns of studied catalysts were examined using a Bruker-D8 advance diffractometer (Figure 3.2) employing CuKα radiation (λ= 1.5406 Å). The diffractometer operated at 40 kV and 40 mA with a scanning rate of 0.1° min^{-1}. The data were collected from 2-theta (2θ) in the range of $0.5\text{-}8.0^{\circ}$ and 10 to 80° for the small-angle and the wide-angle XRD patterns, respectively.

Figure 3.2 Bruker-D8 advance.

3.5.2 Nitrogen adsorption/desorption analysis

Nitrogen (N_2) adsorption/desorption isotherms for SBA-15 and V_xO_y/SBA-15 catalysts were measured by using Micromeritics ASAP 2020 (Figure 3.3). The sample was degassed to vacuum at 300 °C for 1 h under N_2 atmosphere to remove the adsorbed moisture before measurement. The Brunauer-Emmett-Teller (BET) equation was used to calculate the surface area (S_{BET}), while the Barrett-Joyner-Halenda (BJH)

method in the adsorption mode was used to estimate the pore size and pore volume of the samples.

Figure 3.3 Micromeritics ASAP 2020.

3.5.3 NH_3-temperture-programed desorption (NH_3-TPD)

To evaluate the acidity of SBA-15 and nV_xO_y/SBA-15 catalysts, NH_3-temperture programed desorption (NH_3-TPD, Belcat-Basic Chemisorption analyzer (BELLCAT II) instrument equipped with a thermal conductivity detector (TCD)) was applied. The sample (0.02 g) was pretreated in the helium (He) atmosphere from room temperature to 600 ^{o}C at a heating rate of 20 ^{o}C min^{-1} before cooling down to 50 ^{o}C. The samples were subsequently exposed to 5 vol% NH_3 in He mixed gas for 30 min to achieve the saturation and He was then used to flush for 30 min. The adsorbed NH_3 was desorbed in the pure He atmosphere by increasing the temperature in the range of 50-800 ^{o}C at a heating rate of 10 ^{o}C min^{-1}. The amount of desorbed NH_3 from the sample was detected by TCD.

3.5.4 Hydrogen-temperature programed reduction (H_2-TPR)

The reduction temperature of nV_xO_y/SBA-15 catalysts was analyzed by using hydrogen-temperature programed reduction (H_2-TPR) technique (BALLCAT II instrument) and the H_2 consumption was also monitored by using TCD. Before analysis, the catalyst sample was pretreated at 500 $^\circ$C for 30 min in the presence of pure argon (Ar) and cooled down to 50 $^\circ$C. Then, 5 vol% H_2 in Ar mixed gas was introduced to the sample cell during heating from 50 to 900 $^\circ$C at a heating rate 10 $^\circ$C min^{-1}.

3.5.5 X-ray photoelectron spectra (XPS)

The X-ray photoelectron spectra (XPS) of the catalysts were performed on a Kratos Axis ultra DLD spectrometer (Japan) using monochromatic Al Kα (hv= 1486.6 eV) as the X-ray source. The binding energy (BE) of C1s located at 284.6 eV was used as the standard for the correction. The results were analyzed by the Origin program, which uses the Gaussian method.

3.5.6 Transmission electron microscopy (TEM)

The morphology of SBA-15 and nV_xO_y/SBA-15 catalysts were attested by transmission electron microscopy (TEM) with an energy dispersive X-ray (EDX) spectroscope performed on a JEOL JEM- 2100 Plus and JEOL Large Angle SSD at an accelerating voltage of 200 kV. The samples were dispersed in ethanol under sonication. A few drops of the dispersion were placed onto a carbon–coated copper grid followed by solvent evaporation in air at room temperature.

3.6 Characterization of products obtained from the ODH process

3.6.1 Characterization of liquid products

The amount of unreacted OA in the liquid products was evaluated by using gas chromatography flame ionization detector (GC-FID) (Agilent 7890A) contain HP-5 column (ϕ = 0.32 mm; L = 30 m; film thickness = 0.25 μm). The OA conversion could be calculated from the OA calibration curve prepared by using different OA concentrations. The chemical species found in the liquid products were identified using a Shimadzu 2023 Series (Japan) GC System equipped with Shimadzu QP2020 NX (Japan) mass spectrometry (MS) detector and a DB-5 column (ϕ = 0.25 mm; L = 30 m; film thickness = 0.25 μm with a polyethylene glycol stationary phase, Agilent, USA). The measurement was performed at a split ratio of 100:1 using He as a carrier gas at a flow rate of 3 mL min^{-1} and the temperature of injector and detector was controlled at 250 $^{\circ}$C and 300 $^{\circ}$C, respectively. Approximately, the 1.0 μL solution prepared by dissolving 0.1 g sample in 2 mL ethyl acetate was injected into the GC-MS, which the oven temperature was started from 50 $^{\circ}$C and hold at this temperature for 3 min before ramping to 150 $^{\circ}$C at a heating rate of 5 $^{\circ}$C min^{-1} and hold at this point for 10 min. The oven temperature was then increased to 300 $^{\circ}$C at a heating rate of 10 $^{\circ}$C min^{-1} and hold for 20 min. The product selectivity was obtained from the percentage of relative peak area in GC-MS chromatograms.

3.6.2 Characterization of gas products

The gas products were analyzed by using gas chromatography (GC, Shimadzu 2014) equipped with both TCD using a Unibead-C packed column (ϕ = 3 mm; L= 2 m) and flame ionization detector (FID) using a Hayesep-Q column (ϕ = 0.25 mm; L= 2 m; film thickness = 0.25 μm) to evaluate carbon oxides and the rest of the light hydrocarbons, respectively. The amounts of all gaseous products were compared with the standard gases. The GC-FID program was programmed by the GC oven initial

temperature was starting at 50 °C and hold for 5 min. Then, the temperature was increased to 200 °C with a heating rate of 10 °C min^{-1} and hold for 10 min. The sample was injected with a controlled volume of 30 mL using a syringe.

For the evaluation of the amounts of H_2, CO, and CO_2, the gas chromatography thermal conductivity detector (GC-TCD) oven was initially started at 50 °C and hold for 3 min. Then, the temperature was increased to 180 °C with a heating rate of 30 °C min^{-1} and hold for 3 min. The sample was injected with a controlled volume of 60 mL using a syringe.

3.6.3 Determination of coke deposition

The amount of solid product or coke deposited on the surface of the spent catalysts obtained after ODH process were evaluated by using Thermalgravimetric analysis (Perkin Elmer, TGA 8000), as shown in Figure 3.4. The spent catalyst (2 mg) was loaded in a ceramic pan and heated from 30 to 900 °C at a ramp rate of 10 °C min^{-1} under an air atmosphere with a flow rate of 50 mL min^{-1}. The weight loss between 200 and 700 °C was attributed to coke. The weight percentage of coke content was converted to mass per 100 g fresh catalyst.

Figure 3.4 Perkin Elmer-Thermogravitic analyzer (TGA 8000).

CHAPTER IV
RESULTS AND DISCUSSION

This chapter shows the results of catalyst characterization and the catalyst performance to convert OA and the selectivity to long-chain bio-olefins in the liquid and gaseous products via the ODH reaction, which operated through various parameters such as vanadium content (0.5-5.0 wt%), reaction temperature (400-550 °C), catalyst stability (2, 6, 8 h), and catalyst reusability, respectively.

4.1 Catalysts characterization

4.1.1 XRD diffraction

Figure 4.1a shows the small-angle XRD patterns of SBA-15 and nV_xO_y/SBA-15 catalysts. SBA-15 exhibited three diffraction peaks at 2θ of 0.86, 1.49 and $1.68°$ attributed to (100), (110) and (200) planes, respectively. These positions were close to the observation reported by Mitran et al. [12]. These peaks confirmed that the characteristics of SBA-15 was hexagonal symmetry. After vanadium impregnation, the XRD patterns of nV_xO_y/SBA-15 catalysts were similar to that of the original SBA-15, suggesting that the hexagonal ordered structure of SBA-15 was retained. However, it was observed that the 2θ of (100) plane for nV_xO_y/SBA-15 catalysts were shifted towards the higher values in the range of 0.89-0.91 (lower d- values), conveying a change in the distance between the pores. The impregnation of vanadium decreased the values of d_{100}-spacing and unit cell parameter (α_0) of SBA-15 from 10.3 to 9.7 mm and 11.8 to 10.2 nm, respectively when the vanadium loading increased to 5.0 wt%, as shown in Table 4.1. The reduction of d_{100}-spacing possibly resulted from the shrinking of the lattice as a result of condensation after vanadium incorporation and calcination [43]. This corresponds to the pore size of the catalyst being increased after impregnation with the vanadium content. Moreover, it was also observed that the peak intensity of the (100) plane in the nV_xO_y/SBA-15 catalysts tended to be decreased with increasing the

vanadium content. This was due to the formation of partial blocking of mesopores in SBA-15, which could decrease the long-range order of the hexagonal porosity [12, 44]. However, the HRTEM images illustrated in Figure 4.2 exhibited the remaining of the hexagonal arranged porosity, suggesting that the SBA-15's framework was not degraded by vanadium incorporation as described by Liu et al. [43]. Thus, the continuously lower intensity of the nV_xO_y/SBA-15 catalysts with the higher vanadium loading was resulted from the dilution of silica with continuous incorporation of vanadium as a consequence of higher absorption factor for X-rays than silicon [43]. A similar phenomenon was also previously reported for the palladium oxides distributed over the intra-surface of SBA-15 [45].
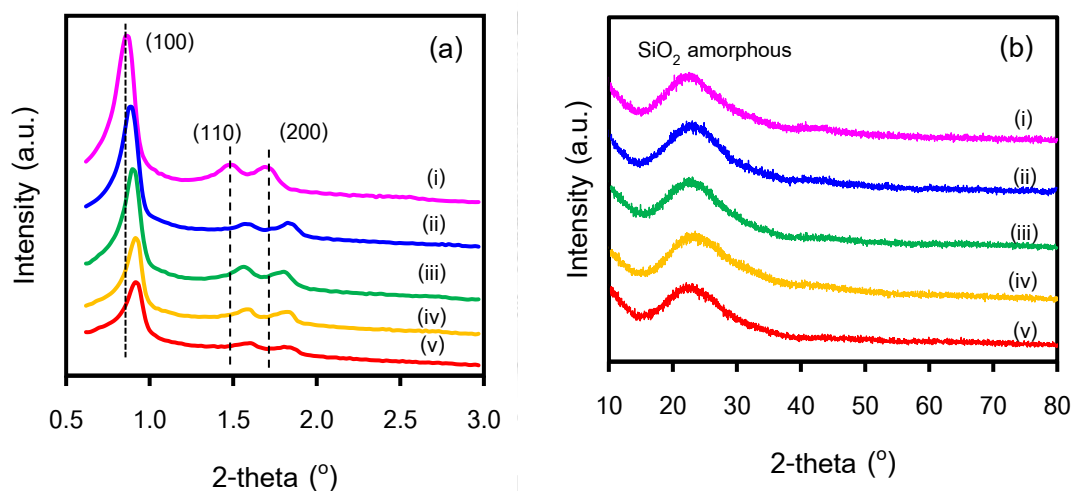
Figure 4.1 XRD patterns of SBA-15 and nV_xO_y/SBA-15 catalysts: (a) small-angle and (b) wide-angle XRD patterns of (i) SBA-15, (ii) 0.5%V_xO_y/SBA-15, (iii) 1.0% V_xO_y/SBA-15, (iv) 3.0%V_xO_y/SBA-15 and (v) 5.0% V_xO_y/SBA-15 catalysts.

Table 4.1 Textural properties, d_{100}-spacing and unit cell parameter of the SBA-15 and nV_xO_y/SBA-15 catalysts

Sample	d_{100}[a] (nm)	α_0[b] (nm)	S_{BET}[c] ($m^2 g^{-1}$)	Pore size[d] (nm)	Pore volume[e] ($cm^3 g^{-1}$)
SBA-15	10.3	11.8	912	5.26	1.07
0.5%V_xO_y/SBA-15	9.92	11.4	839	5.27	1.03
1.0%V_xO_y/SBA-15	9.92	11.4	707	5.16	0.92
3.0%V_xO_y/SBA-15	9.70	10.2	684	5.55	0.84
5.0%V_xO_y/SBA-15	9.70	10.2	575	5.45	0.79

[a] d_{100}-spacing, calculated from the low angle of XRD patterns using Bragg's equation: $\lambda=2dsin\theta$ [46];

[b] XRD unit-cell parameter, estimated from the position of the (100) diffraction line ($\alpha_0=2d_{100}/\sqrt{3}$) [47];

[c] BET surface area; [d] BJH adsorption average pore size; [e] BJH adsorption cumulative volume of pores.

From the wide-angle XRD patterns depicted in Figure 4.2b, SBA-15 and nV_xO_y/SBA-15 catalysts exhibited a broad peak at 2θ of 20-30° assigned to the amorphous silica. However, no diffraction peaks corresponding to V_2O_5 crystalline for nV_xO_y/SBA-15 catalysts were observed, suggesting the well-dispersed of the vanadium oxides on the SBA-15 surface, likely as mono- (VO_4^{3-}) and polyvanadate species (V_xO_y) [12].

4.1.2 Morphology of SBA-15 and nV_xO_y/SBA-15 catalysts

The morphology of SBA-15 and nV_xO_y/SBA-15 catalysts were analyzed by the high-resolution TEM (HRTEM), as shown in Figure 4.2. The HRTEM images of all samples indicated the well-order hexagonal arrays of mesopores [43] and clearly observed that the ordered mesoporous structure of SBA-15 was preserved after loading the vanadium oxide. However, the cluster or particles of V_xO_y for nV_xO_y/SBA-15 catalysts were not observed even though the high vanadium loading was applied. This implied that the particles of vanadium species were highly dispersed over the mesopore intra-surface [48]. To confirm the presence of vanadium species in the prepared catalysts, the EDX mapping by TEM analysis of the nV_xO_y/SBA-15 catalysts (Figure 4.3). The

results indicated the well-dispersion of vanadium species located in the internal pore of the catalysts. This information was consistent with the results attested by XRD and N_2 adsorption-desorption analyses. The observation was also similar to the previous literatures, which prepared vanadium oxide on SBA-15 via wet impregnation and founds the vanadium in the internal pore of the catalyst [43, 49].
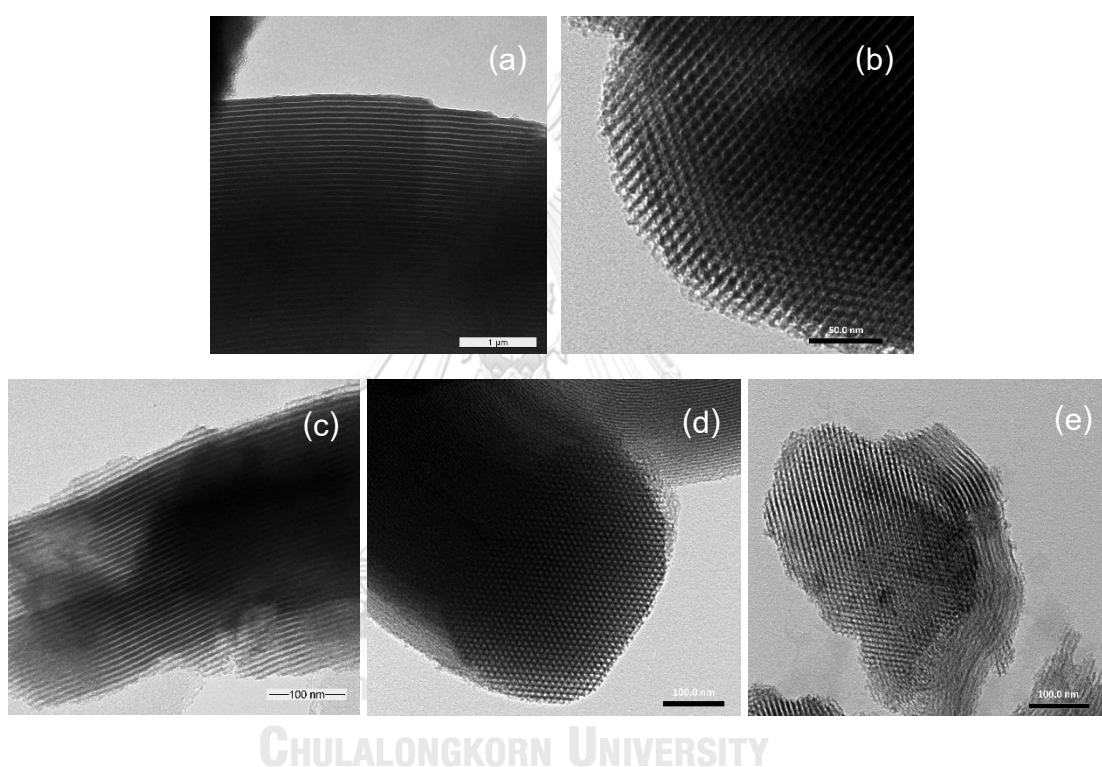
Figure 4.2 HRTEM images of (a) SBA-15, (b) 0.5%V_xO_y/SBA-15, (c) 1.0%V_xO_y/SBA-15, (d) 3.0% V_xO_y/SBA-15, and (e) 5.0% V_xO_y/SBA-15 catalysts.
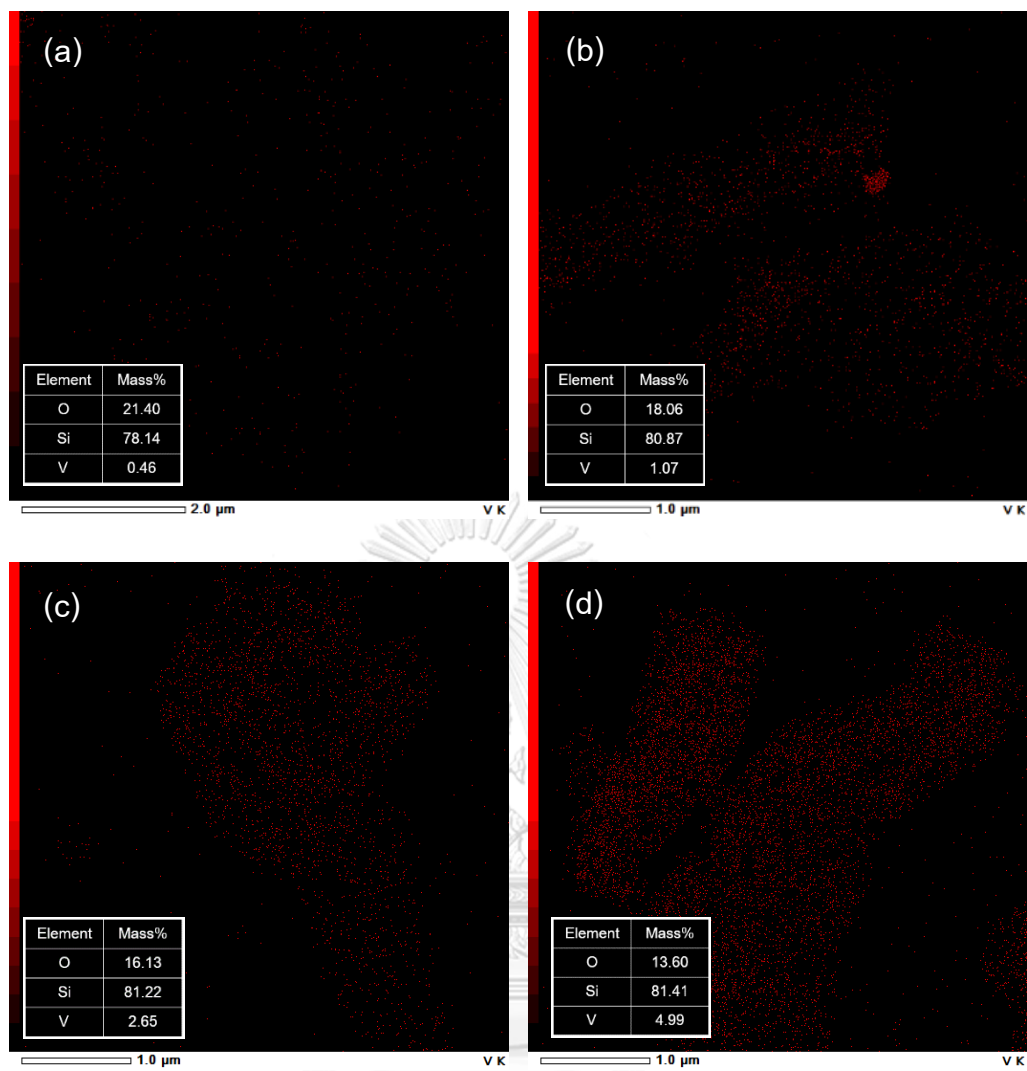
Figure 4.3 TEM-EDX elemental mapping vanadium of (a) 0.5%V_xO_y/SBA-15, (b) 1.0%V_xO_y/SBA-15, (c) 3.0%V_xO_y/SBA-15, and (d) 5.0% V_xO_y/SBA-15 catalysts.

4.1.3 Textural properties of SBA-15 and nV_xO_y/SBA-15 catalysts

The N_2 adsorption-desorption isotherms of SBA-15 and nV_xO_y/SBA-15 catalysts were showed in Figure 4.4a. All samples exhibited type IV isotherms with H1 hysteresis loop, which is the typical characteristics of mesoporous structure with cylindrical pores, according to IUPAC classification [50]. The sharp reflection of the hysteresis loop appeared in the isotherms between the relative pressure (P/P_o) in the range of 0.6-0.8. It was corresponded to the effect of capillary condensation due to the uniform mesoporosity [51]. The textural properties of the SBA-15 and nV_xO_y/SBA-15 catalysts were summarized in Table 4.1. The result showed that SBA-15 had high surface area of 912 m^2 g^{-1}, with the pore volume and pore size of 1.07 cm^3 g^{-1} and 5.26 nm, respectively. The impregnation of the higher vanadium contents to 5.0 wt% onto SBA-15 remarkably decreased the surface area and pore volume to 575 m^2 g^{-1} and 0.79 cm^3 g^{-1}, respectively. This reflected that the V_xO_y particles deposited on the pore wall and partially blocked the pores of SBA-15 support. On the other hand, there were no significant change of the pore size and very narrow pore-size distribution were still remained in the range of 5.16-5.45 nm as shown in Figure 4.4b. This indicated that the V_xO_y particles were well uniformly dispersed and deposited inside the pores of SBA-15 support, which was consistent with the XRD results.
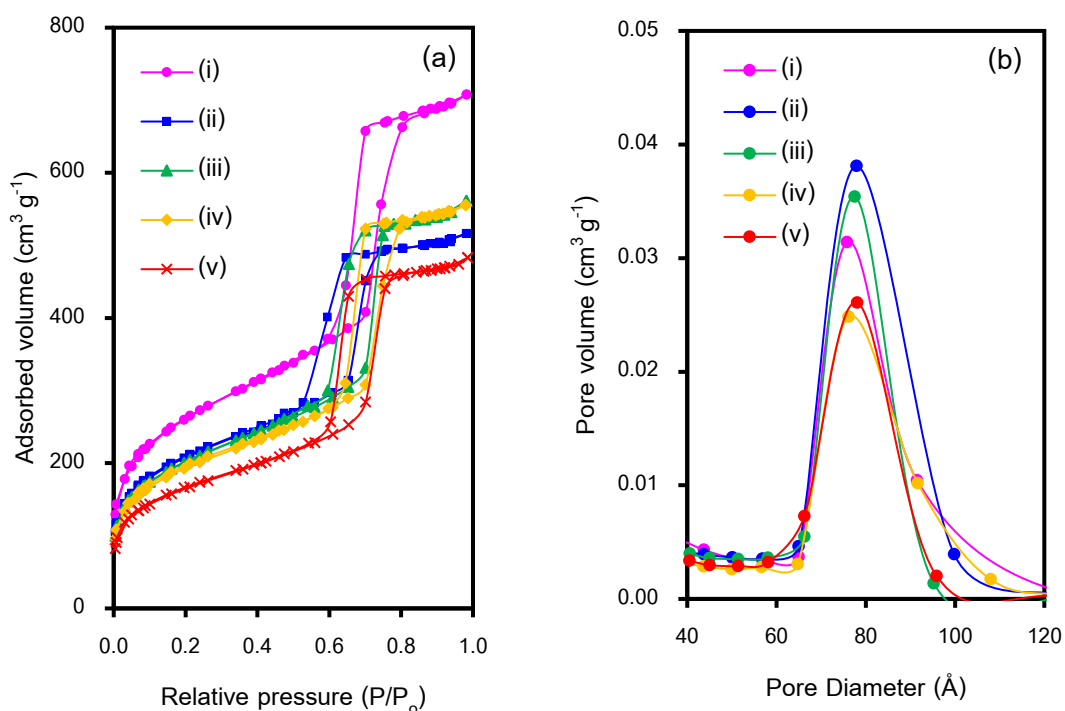
Figure 4.4 Representative (a) N_2 adsorption-desorption isotherms and (b) pore size distribution of the (i) SBA-15, (ii) 0.5%V_xO_y/SBA-15, (iii) 1.0% V_xO_y/SBA-15, (iv) 3.0%V_xO_y/SBA-15, and (v) 5.0% V_xO_y/SBA-15 catalysts.

4.1.4 X-ray photoelectron spectra (XPS)

The XPS technique was applied to distinguish the surface oxidation states and the chemical environment of vanadium species. As illustrated in Figure 4.5, the XPS spectra of V2p for all catalysts were broad in the range of 514-520 eV except that of 0.5%V_xO_y/SBA-15 catalyst, which the concentration of vanadium was below to the detection limit for the XPS analysis. After deconvolution of V2p peak, the broad peak at this signal was consisted of two components at the binding energy (BE) of 516 and 517 eV attributed to the oxidation states for V^{4+} in VO_2 and V^{5+} in the V_2O_5 species, respectively [52, 53]. The percentage of V^{4+} and V^{5+} to the total vanadium species was also calculated as shown in Table 4.2. It was noticed that the major oxidation state of vanadium species in the catalysts having 1.0-3.0 wt% vanadium content was V^{4+}

species with the percentage of the relative peak area as 75.3-95.6%. The amount of V^{4+} species decreased to 28.1% with increasing the vanadium content to 5 wt%. At this point, the amount of V^{5+} species increased to 71.9% and became the major oxidation state. This implied that the increase in the vanadium content possibly changed the dominant formation of vanadium species on the surface of SBA-15 by aggregation of vanadium to slightly shift towards the higher BE value [13].
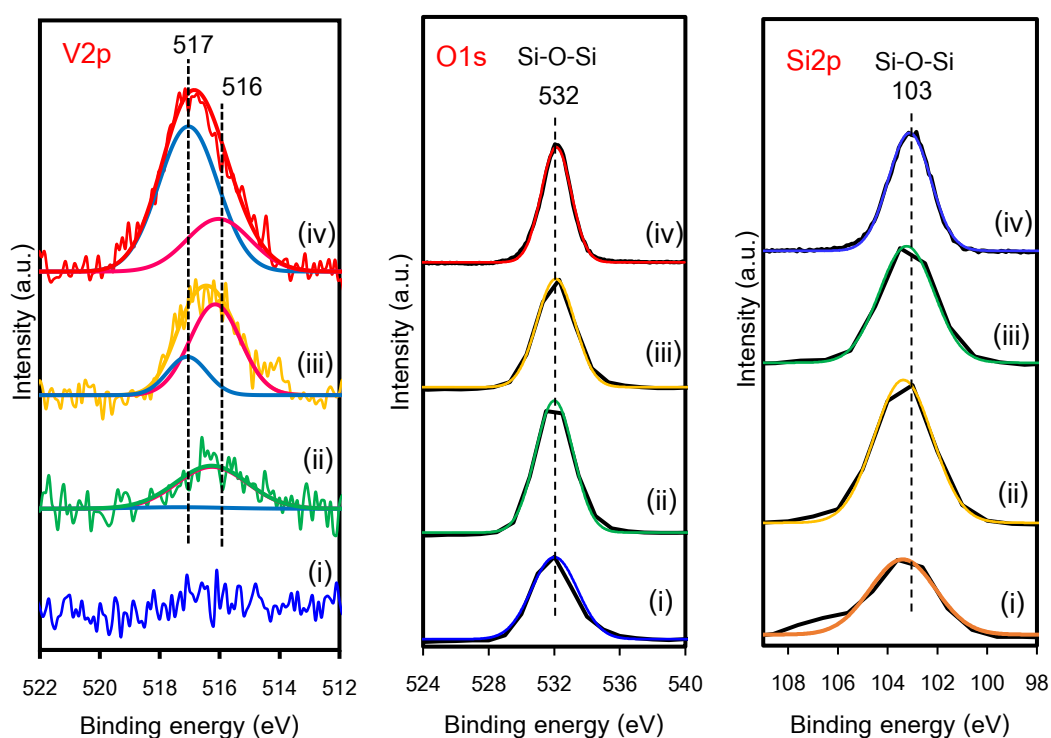
Figure 4.5 XPS spectra for V2p$_{3/2}$ signals of the (i) 0.5%V$_x$O$_y$/SBA-15, (ii) 1.0% V$_x$O$_y$/SBA-15, (iii) 3.0%V$_x$O$_y$/SBA-15, and (iv) 5.0% V$_x$O$_y$/SBA-15 catalysts.

Table 4.2 XPS data of prepared nV_xO_y/SBA-15 catalysts

Catalysts	Peak area (%)		O1s	Si2p
	516 eV (V^{4+})	517 eV (V^{5+})	(eV)	(eV)
0.5%V_xO_y/SBA-15	n.d.	n.d.	532.0	103.4
1.0%V_xO_y/SBA-15	95.6	4.4	532.0	103.4
3.0%V_xO_y/SBA-15	75.3	24.7	532.1	103.2
5.0%V_xO_y/SBA-15	28.1	71.9	532.1	103.2

n.d. = not be detected.

The Si2p and O1s signals of all catalysts centered at the BE of 103 and 532 eV, respectively. They were corresponded to Si-O-Si bond from silica [54]. This BE value at 532 eV was close to the BE of SBA-15 (533 eV). This implied that the BE 532 eV should be attributed from Si-O-Si bond rather than oxygen atom in V_2O_5 nanostructure, which is normally appeared at the BE of 530.2 eV [13, 55]. This indicated that the O1s signal of catalysts were mainly reflected from SBA-15, suggesting that the most of the loaded vanadium species were deposited inside the SBA-15 pores. This result was also consistent with the data obtained from XRD and TEM analyses that the V_2O_5 crystallite diffraction peak and V_2O_5 particles on the surface of catalysts were not observed. This confirmed the well-dispersed vanadium particles on to the surface of SBA-15 support. Moreover, the BE of Si2p showed in the range of SiO_2 (103.0-103.5 eV). This indicates that the structure of SBA-15 has not significantly changed after vanadium loading.

4.1.5 NH_3-temperture-programed desorption (NH_3-TPD)

The acidity of catalysts was measured by using NH_3-TPD analysis, as shown in Figure 4.6a. The type of acidic sites was classified from the desorption temperature of the adsorbed ammonia in each catalyst. The amounts of ammonia desorption appeared at the range of 100-250 ^{o}C and 250-400 ^{o}C were denoted as weak and medium acid sites, respectively [56]. The NH_3-TPD profile of SBA-15 exhibited the

NH_3-desorption peak at 78 ^{o}C, which related to the very weak acid sites [13]. For nV_xO_y/SBA-15 catalysts, the NH_3-TPD profiles exhibited two NH_3-desorption peaks partially overlapping in the range 50-350 ^{o}C. The first signal appeared at 50-200 ^{o}C was the weak acid sites attributed to the isolated tetrahedral-like coordinated V_xO_y species [57], whereas the second one located at the higher desorption temperature (200-350 ^{o}C) was the medium acid sites. With increasing the vanadium content, the intensity of weak acid desorption peaks dramatically increased and slightly shifted to the higher desorption temperatures, while medium acid desorption peaks softly increased. This implies that the increased vanadium content has affected the catalyst acidity. The total acidity increased from 168 to 814 µmol g^{-1} when the vanadium content increased from 0.5 to 5.0 wt% as shown in Table 4.3.
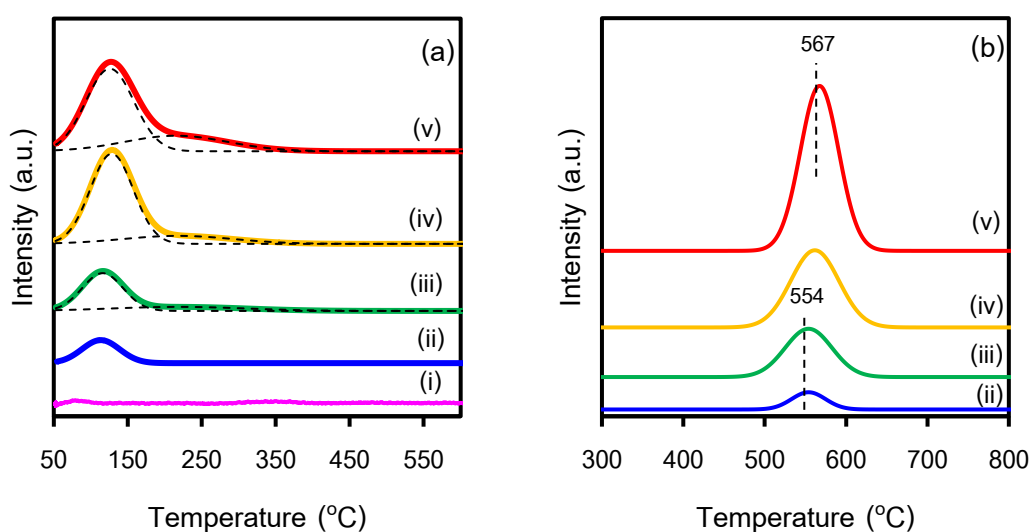
Figure 4.6 Representative (a) NH_3-TPD profiles and (b) H_2-TPR profiles of the (i) SBA-15, (ii) 0.5%V_xO_y/SBA-15, (iii) 1.0% V_xO_y/SBA-15, (iv) 3.0%V_xO_y/SBA-15, and (v) 5.0%V_xO_y/SBA-15 catalysts.

Table 4.3 Surface properties of SBA-15 and nV_xO_y/SBA-15 catalysts

Catalysts	NH$_3$-TPD			H$_2$-TPR	
	$(\alpha)^a$ (µmol g^{-1})	$(\beta)^b$ (µmol g^{-1})	Total acidity (µmol g^{-1})	T_M (^{o}C)	H$_2$ consumption (µmol/g)
SBA-15	32	27	59	-	-
0.5%V$_x$O$_y$/SBA-15	145	23	168	554	40
1.0%V$_x$O$_y$/SBA-15	239	19	258	554	140
3.0%V$_x$O$_y$/SBA-15	518	36	554	561	260
5.0%V$_x$O$_y$/SBA-15	737	77	814	567	610

^{a}Weak acid site; ^{b}Medium acid site; ^{c}Peak temperature (T_M)

4.1.5 H$_2$-temperture-programed reduction (H$_2$-TPR)

The profile of reduction temperature of vanadium oxides supported on SBA-15 support was also determined using H$_2$-TPR analysis as shown in Figure 4.6b. The details of peak temperature and H$_2$-consumption were summarized in Table 4.3. It was observed only one sharp reduction peak for all nV_xO_y/SBA-15 catalysts. The nV_xO_y/SBA-15 catalysts containing 0.5-1.0 wt% V_xO_y loading had the reduction temperature at ca. 554 ^{o}C. and it was shifted to the higher value at 567 ^{o}C when the vanadium content increased to 5.0 wt%. The peak at lower temperature attributed to the reduction of monomeric (V^{4+}, VO_2) and oligomeric (V^{5+}, VO_4^{3-})$_n$ species in the tetrahedral coordination geometry [12, 13, 43]. However, the reduction peak or shoulder peak at the higher reduction temperature at ca. 590-600 ^{o}C attributed to the reduction of polymeric V^{5+} species in V_2O_5 crystalline was not appeared. This implied that the nV_xO_y/SBA-15 catalysts were mainly consisted of the monomeric and oligomeric vanadium species. This observation was consistent with the XRD and XPS analysis. Notably, the reduction peak intensity was increased and gradually shifted to the higher temperature when the vanadium content increased. This implied the formation of less reducible high polymeric vanadium species.

4.2 Catalytic testing for the ODH of OA

4.2.1 Effect of the various vanadium contents in nV_xO_y/SBA-15 catalysts

The catalytic performance of nV_xO_y/SBA-15 catalysts for ODH of OA was performed by using 0.2 g catalyst loading at 450 ^{o}C under the OA and O_2/N_2 (1/1 (v/v)) feed rates at 0.1 mL min^{-1} and 100 mL min^{-1}, respectively. The results shown in Table 4.4 indicated that the catalytic performance for OA conversion was strongly depended on the vanadium content. All catalysts had high performance to promote ODH and achieved more than 75% OA conversion. Without the addition of vanadium, the high S_{BET} area and large pore volume of SBA-15 could facilitate the diffusion of reactants and might promote the undesired cracking of OA to achieve 76.7% OA conversion [19, 58]. For the nV_xO_y/SBA-15 catalysts. The 1.0%V_xO_y/SBA-15 catalyst exhibited the highest performance to achieve 83.7% OA conversion. Above this point, the OA conversion gradually decreased with increasing the vanadium content. This result was related to the textural properties of the catalysts as shown in Table 4.1 and implied that the high loading of vanadium dramatically decreased both surface area and pore volume of the catalyst to yield the lower catalytic activity. To consider the product distribution obtained from the reaction in terms of liquid, gas, and solid products as exhibited in Table 4.4, it was observed that the amount of solid product was less than 0.2 wt% for all applied condition reflecting that the coke formation on the surface of nV_xO_y/SBA-15 was inhibited. A proportion of products were also influenced by the vanadium loading on SBA-15 catalyst. When the vanadium content increased to 5.0 wt%, the amount of liquid product decreased from 79.0 to 68.5 wt% with increasing the portion of gas product from 20.9 to 31.4 wt%. This was possibly due to the effect of higher acidity induced by the higher vanadium loading (Table 4.3) and yielded the catalysts having higher potential to encourage the secondary cracking and deep oxidation to generate the high content of gaseous products [59, 60].

Table 4.4 Effect of vanadium content and reaction temperature on the conversion level and product distribution obtained from ODH of OA

Catalysts	Reaction Temperature ($^{\circ}$C)	OA conversion (%)	Product distribution (wt%)		
			Liquid	Gas	Solid
SBA-15	450	76.6 ± 1.78	79.0 ± 0.66	20.9 ± 0.06	0.10 ± 0.60
0.5%V$_x$O$_y$/SBA-15	450	77.7 ± 1.64	76.3 ± 3.50	23.7 ± 0.02	0.04 ± 3.48
1.0%V$_x$O$_y$/SBA-15	450	83.7 ± 2.54	75.5 ± 4.14	24.4 ± 0.11	0.10 ± 4.03
3.0%V$_x$O$_y$/SBA-15	450	82.3 ± 0.77	75.3 ± 0.76	24.7 ± 0.00	0.03 ±0.75
5.0%V$_x$O$_y$/SBA-15	450	79.2 ± 2.53	68.5 ± 0.15	31.4 ± 0.00	0.10 ± 0.15
1.0%V$_x$O$_y$/SBA-15	400	46.4 ± 0.44	71.7 ± 0.12	28.2 ± 0.00	0.10 ± 0.12
1.0%V$_x$O$_y$/SBA-15	500	81.4 ± 0.13	68.5 ± 0.46	31.5 ± 0.00	0.04 ± 0.47
1.0%V$_x$O$_y$/SBA-15	550	80.5 ± 0.42	53.9 ± 1.50	46.1 ±0.02	0.05 ± 1.48

To investigate the selectivity in the liquid products obtained from ODH of OA, the liquid products were consisted of two phases; organic and aqueous phase. After the separation of aqueous product, the chemical species in the organic phase were analyzed by GC-MS technique. The compositions in the organic products were classified into 5 groups such as alkanes, alkenes, aromatics, cyclics, and oxygenated compounds. The cyclic compounds were consisted of cycloalkanes and cycloalkenes, while the oxygenated compounds involved with alcohols, aldehydes, ketones, carboxylic acids, and esters. Figure 4.7 shows the effect of vanadium loading in the nV$_x$O$_y$/SBA-15 catalysts on the product selectivity in the organic phase of the liquid product obtained from ODH of OA operated at 450 $^{\circ}$C for 2 h at ambient pressure. It was seen that olefins or alkenes and oxygenated compounds were primary products. Without the vanadium impregnation, the ODH of OA catalyzed by only SBA-15 provided the liquid product mostly containing 43.2% and 40.3% selectivity to olefins and oxygenated compounds, respectively with small amounts of alkanes, cyclics and aromatics. The α-alkenes/total alkenes ratio was calculated as 0.26, which the total

alkenes were consisted with dienes, trienes, tetraenes, and internal alkenes. These results might be attributed to the basic nature of SBA-15. According to the high surface area and pore volume with a quite large pore size of SBA-15, these textual properties were advantageous to the ease of diffusion of substate molecules and consequently promoted the decarboxylation, decarbonylation [61], or dehydration [62, 63] of OA. When 0.5%V_xO_y/SBA-15 was applied for ODH of OA, the liquid product containing the lower content of the oxygenated species with increasing the amounts of aromatics and cyclics. This was possible that the presence of monomeric vanadium species (VO_2) in the catalyst were active to produce alkenes via dehydration during ODH [64]. These alkenes might be further acted as the precursors to produce aromatics [9]. In addition, cyclic fatty acid monomer (CFAM) or cyclization of OA could be formed during heating reaction temperature at 200 $^\circ$C and above [65, 66]. When the amount of vanadium loading increased to 3.0 wt%, the selectivity to olefins decreased with higher selectivity to aromatics and oxygenated compounds. This could be explained that the increasing vanadium loading, which exhibited the higher acidity, could promote the cracking of long-chain olefins to produce alkanes and internal alkene radicals that promoted the formation of aromatic compounds [67]. Notably, the α-alkenes/total alkenes ratio was highest at 0.58 when 3.0%V_xO_y/SBA-15 catalyst was applied under the given reaction condition. This might be related to the acidity of the catalyst. The catalysts with higher acidity could inhibit the desorption of the formed dienes from the catalyst surface, which were further formed as aromatics compounds. Thus, the amount of total alkene was decreased and consequently resulted to the higher α-alkenes/total alkenes ratio.

However, the use of 5.0%V_xO_y/SBA-15 catalyst exhibited the dramatic reduction of α-alkenes/total alkenes ratio to 0.28 and the selectivity to aromatics was also decreased with the greater selectivity to oxygenated compounds. This was due to the overdose of vanadium species that could promote the deep oxidation [12, 13], to generate the higher amount of gaseous products as seen in Table 4.4.
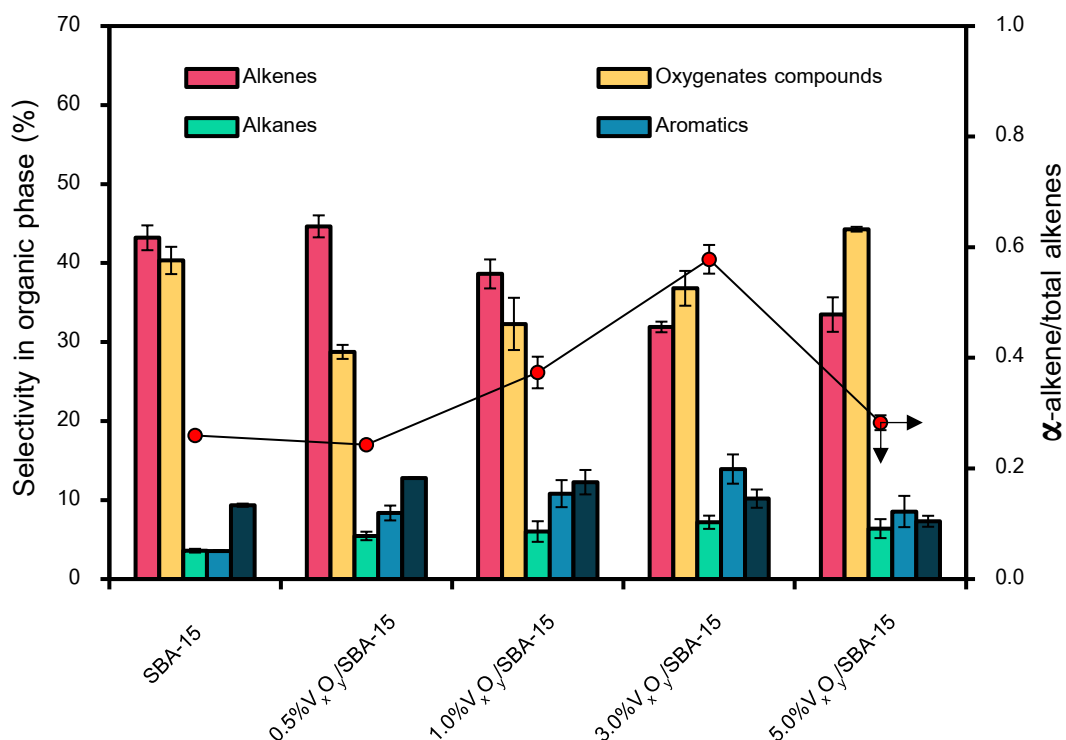
Figure 4.7 Effect of the various vanadium content in the nV_xO_y/SBA-15 catalysts on the selectivity in the organic phase of liquid product and α-alkenes/total alkenes ratio.

Figure 4.8 shows the distribution of carbon atoms in the organic phase of the liquid product obtained from the ODH of OA over nV_xO_y/SBA-15 catalysts at 450 $^\circ$C. The range of carbon atoms was categorized into four groups according to their applications of olefins: C_{5-9} (plastics and polymers), C_{10-14} (surfactants and detergent), C_{15-18} (lubricant oil), and C_{20+} (synthetic waxes) [68, 69]. For the ODH of OA catalyzed by SBA-15, the majority of products was alkenes in the C_{10-14} range, whereas the C_{18+} products were mostly consisted of the oxygenated compounds. Due to the low acidity of SBA-15 catalysts, this property reduced the chance of cracking whereas the coupling reactions to form the larger oxygenated products were possibly promoted. However, the catalyst by impregnation of vanadium oxides (nV_xO_y/SBA-15) exhibited a different majority of alkenes, correlated with the amount of vanadium species on the catalyst surface and their acidity. The results in Figure 4.8 showed that the 0.5-1.0 wt% of

vanadium loading, which having high level of V^{4+} (VO_2) species, provided the alkenes in the range of C_{10-14}. Besides, the increasing vanadium loading over 1.0 wt% decreased the level of alkenes in the range of C_{10-14}. This was possibly due to the rise of catalyst acidity by increasing the vanadium content. The higher acidity could decrease the long-chain alkene via cracking reaction. Furthermore, the increase in the vanadium content from 3.0-5.0 wt% enhanced the ability to induce aromatics formation. This was possibly due to the higher level of V^{5+} (V_2O_5) species that could promote aromatization. [70]. Moreover, the increasing vanadium loading to 5.0 wt.% decreased the selectivity to aromatics with increasing in the selectivity to long-chain oxygenated compounds (C_{18+}), which were mostly consisted of alcohols and aldehydes. These results suggested that the existence of the polymeric V_xO_y species could promote the formation of oxygenated compounds.
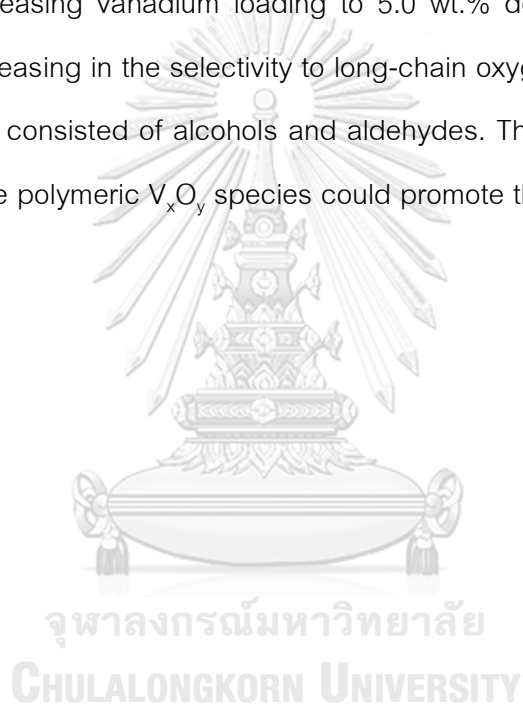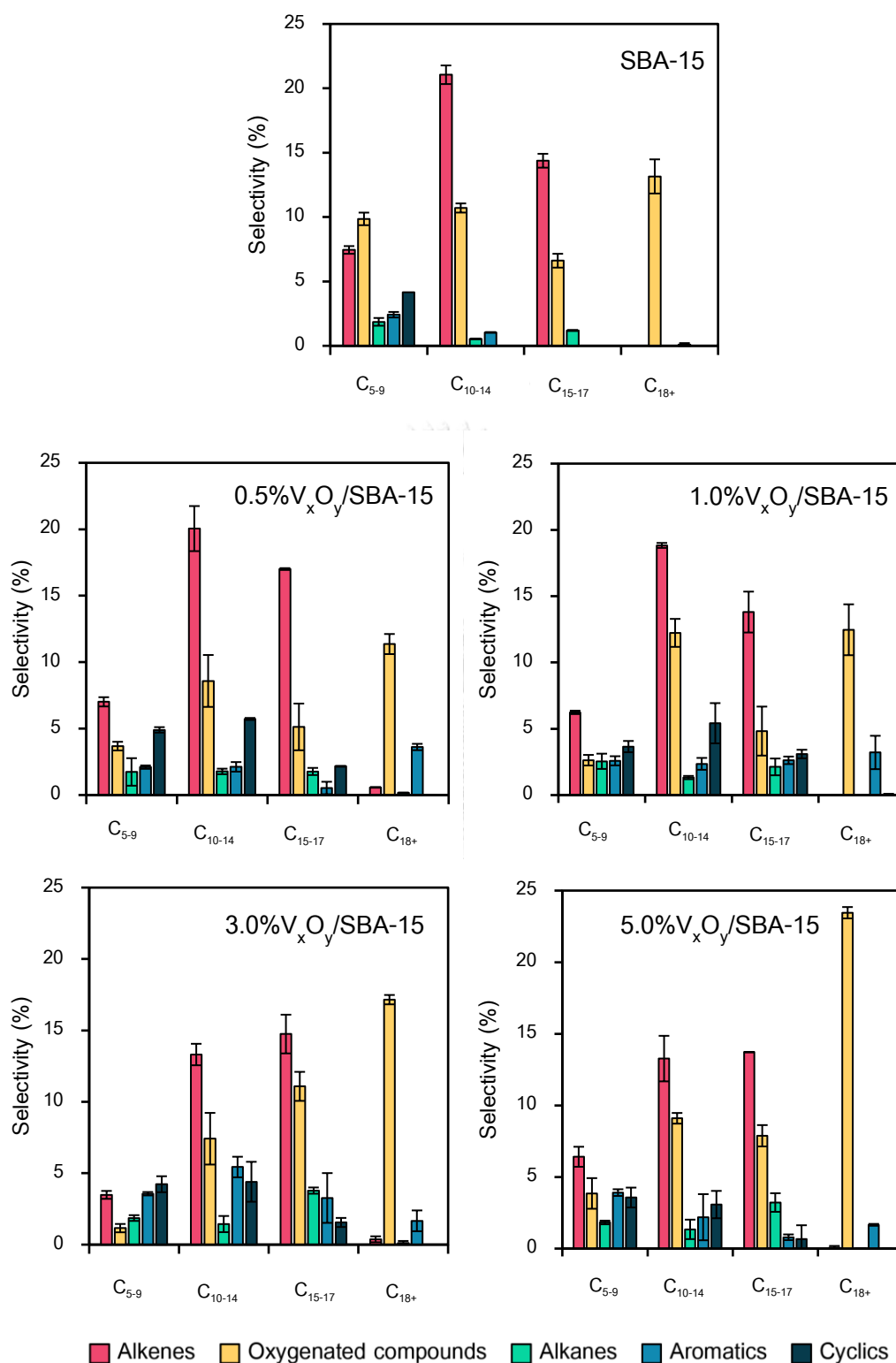
Figure 4.8 Effect of the various vanadium content of nV$_x$O$_y$/SBA-15 catalysts on the distribution of carbon atoms in the organic phase of the liquid product.

From the product analysis, the possible reaction pathway for ODH of OA was proposed in Figure 4.9. The transformation of OA via ODH reaction can be occurred through three pathways: the pathway (1) involved with the decarboxylation (DCO_2) of OA to produce long-chain internal alkenes (8-heptadecene, $C_{17}^=$) and CO_2 as the by-product. Because the C=C bond and -COOH in 8-heptadecene had high electron density, they could be activated by the acidic sites on the catalyst surface for dehydrogenation to generated the new C=C bonds in the chains to obtain dienes or it could be broken down of the C-C bond at the β-position of C=C to produce the short-chain alkanes and alkenes [71-74]. The pathway (2) related the decarbonylation (DCO) to provide the formation of alcohols and aldehydes, followed by dehydration of alcohol and cracking of C-C bonds at β-position of C=C to generate the short-chain hydrocarbons, CO and water [71, 75]. Besides, the pathway (3) might be occurred through the oxidative cleavage at internal C=C bond of OA via epoxidation, which was then hydrolyzed to form diols and finally release a carboxylic acid and water [76-78]. This carboxylic acid could be undergone to DCO_2 and dehydrogantion to produce short-chain alkanes and alkenes. Moreover, the alkenes from all reaction pathways could be used as precursors for futher reactions such as oxidative cleave of alkenes, catalyst cracking, and aromatization to generate the oxygenated compounds (aldehyde and ketone), light olefins and aromatics, respectively [67, 79, 80].
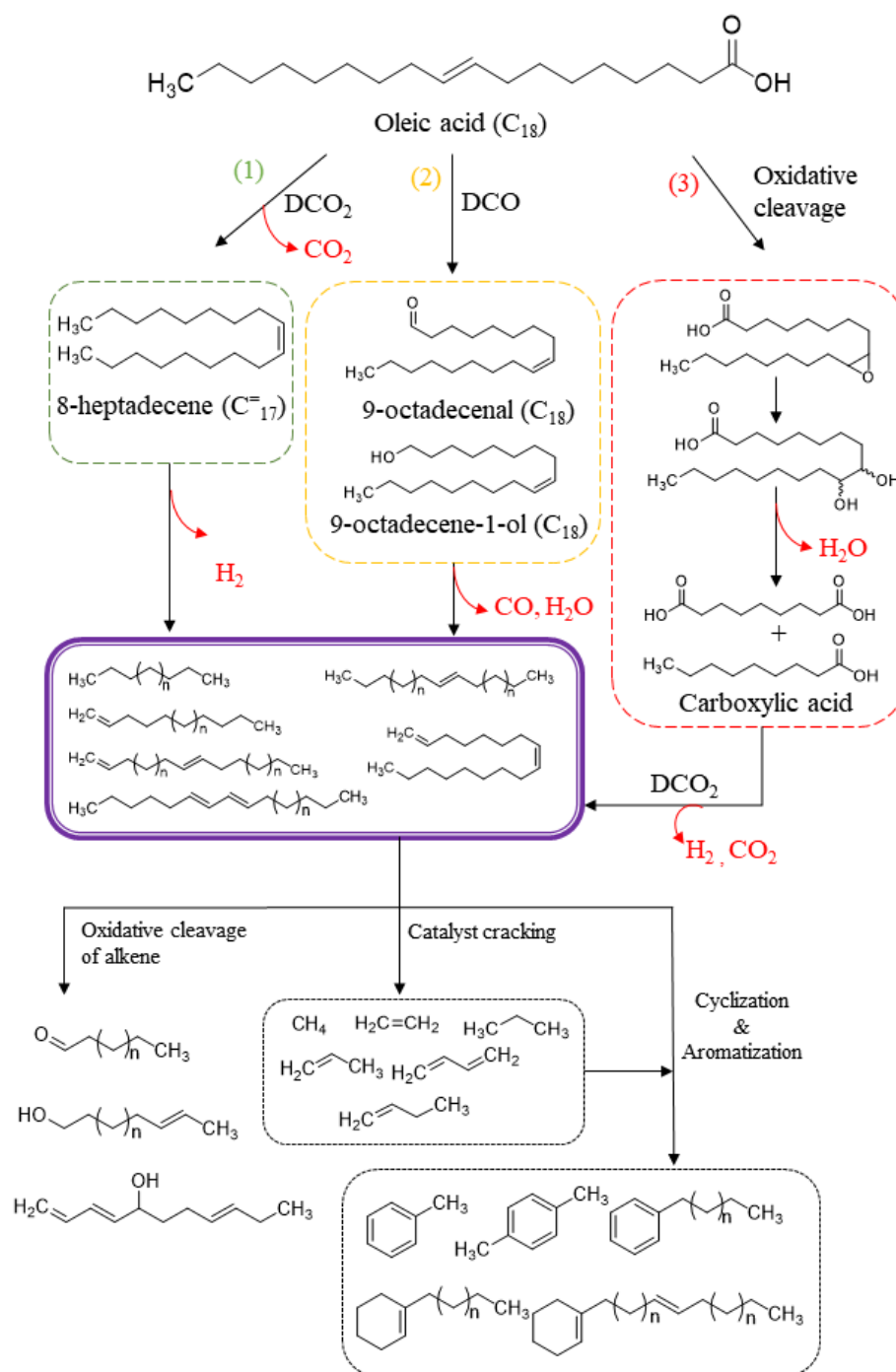
Figure 4.9 Proposed reaction pathway for the ODH of OA over the SBA-15 and nV_xO_y/SBA-15 catalysts.

Figure 4.10 shows the concentration of gas products consisted of hydrogen (H_2), carbon oxides (CO and CO_2), and light hydrocarbons (C_1-C_{4+}). The results indicated that CO_2 was the dominant product, suggesting that the reaction pathway for ODH of OA might be occurred through DCO_2, which was proportional to the vanadium contents. Moreover, the higher acidity induced from the higher vanadium contents could promote the deep oxidation to produce CO_2 as seen that the concentration of CO_2 increased when the vanadium content increased from 0.5 wt.% to 3.0 wt.%. However, the concentration of CO_2 seemed to decrease, with increasing H_2 content was observed when 5.0% V_xO_y/SBA-15 catalyst was applied. This was possible that the catalyst with higher vanadium content had higher acidity to enhance the dehydrogenation activity to produce H_2 during ODH process from 1.07 to 8.46 mol%. Moreover, the overdose vanadium content might also have less activity for deep oxidation to produce the lower CO_2 content with higher amount of CO gas instead.
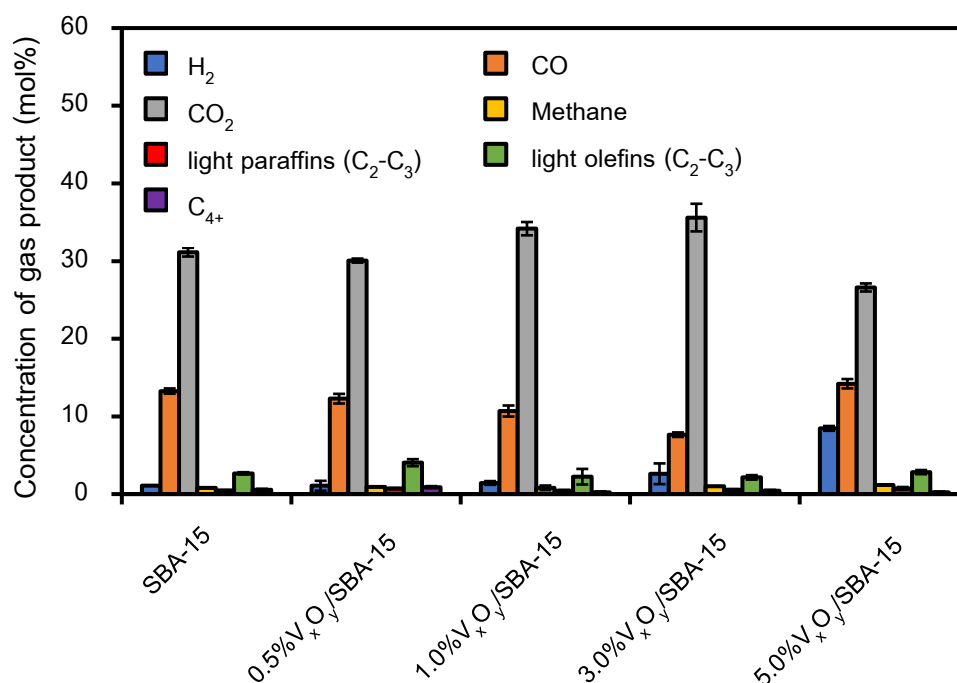
Figure 4.10 Effect of the various amounts of vanadium loading in the nV_xO_y/SBA-15 catalysts on the concentration of gas products obtained from ODH of OA.

4.2.2 Effect of reaction temperature on ODH of OA

In this section, the catalytic testing was carried out over a 1.0%V_xO_y/SBA-15 catalyst at 400-550 $^{\circ}$C for 2 h under the OA and O_2/N_2 (1/1 (v/v)) feed rates at 0.1 mL min^{-1} and 100 mL min^{-1}, respectively. The results from Table 4.4 showed that the appropriate reaction temperature for ODH of OA should be higher than 400 $^{\circ}$C. The applied reaction temperature at 400 $^{\circ}$C provided only 46.4% OA conversion, whereas the higher reaction temperature to 450-550 $^{\circ}$C obtained ca. 80-83% OA conversion. However, the temperature above 450 $^{\circ}$C slightly decreased the OA conversion. This suggested that the reaction temperature at 400 $^{\circ}$C and 2 h was not sufficient to overcome the activation energy of the ODH reaction, whereas the operation at the high reaction temperature (> 450 $^{\circ}$C) decreased the degree of OA conversion due to the exothermic nature of the ODH reaction. Not only the OA conversion, but the reaction temperature also affected the selectivity to the species in the organic liquid phase as shown in Figure 4.11. When the ODH reaction was operated at low temperature (400 $^{\circ}$C), it was observed that the oxygenated compounds was the dominant products. Whereas, the increasing reaction temperature induced the catalyst to have the higher effective for producing alkenes and aromatic compounds with the selectivity of 43.9% and 25.4%, respectively. This was possible that the side reactions such as epoxidation or oxidation cleavage would be promoted to produce oxygenated products at a low reaction temperature [76], while the higher reaction temperature enhanced the selectivity to small molecules or aromatics by consuming the generated alkenes via cracking and aromatization, respectively [9]. However, the increasing reaction temperature from 500 to 550 $^{\circ}$C decreased the alkene selectivity from 43.9% to 33.5% due to the effect of thermal cracking of the alkenes, which enhanced the chance to produce alkyl benzenes. Although the α-alkenes/total alkenes ratio decreased with rising temperature, this ratio increased from 0.31 to 0.45 when the reaction temperature increased to 550 $^{\circ}$C resulting from the increase in the α-alkenes selectivity. This implies

that the reaction temperature below 550 $^{\circ}$C decreased the α-alkenes due to increased catalytic activity for isomerization to produce the internal olefins. Furthermore, the reaction temperatures higher than 500°C promoted the deep ODH of OA to increase the cracking of long-chain alkenes to produce the short-chain α-alkenes with the light olefins in the gas phase. Therefore, the distribution of carbon atoms in liquid products (Figure 4.12) showed the short-chain alkenes (C_{5-9}) increased when the reaction temperature increased from 400 to 500 $^{\circ}$C due to thermal cracking. Moreover, high reaction temperature (>500°C) exhibited a dramatic increase in the aromatic compounds (C_{5-14}) with the reduction of alkenes portion in the liquid product. This suggested that alkenes were the precursors to produce aromatics, especially at high temperatures.

This observation was corresponded to the results of the concentration of the gas products. Figure 4.13 exhibited that the contents of light olefins ($C^{=}_{2-3}$) and light paraffins (C_{2-3}) increased from 1.49 to 5.42 mol% and from 0.26 to 1.49 mol%, respectively, when the reaction temperature increased from 400 to 550 $^{\circ}$C. While the selectivity to carbon oxides showed a gradual decrease as the temperature rises. This was possibly due to the formation of the aromatics, as styrene, ethylbenzene, and xylene, which had a stable aromatic nucleus and thereby reduced the production of carbon oxides, which might be contributed from the secondary combustion [9].
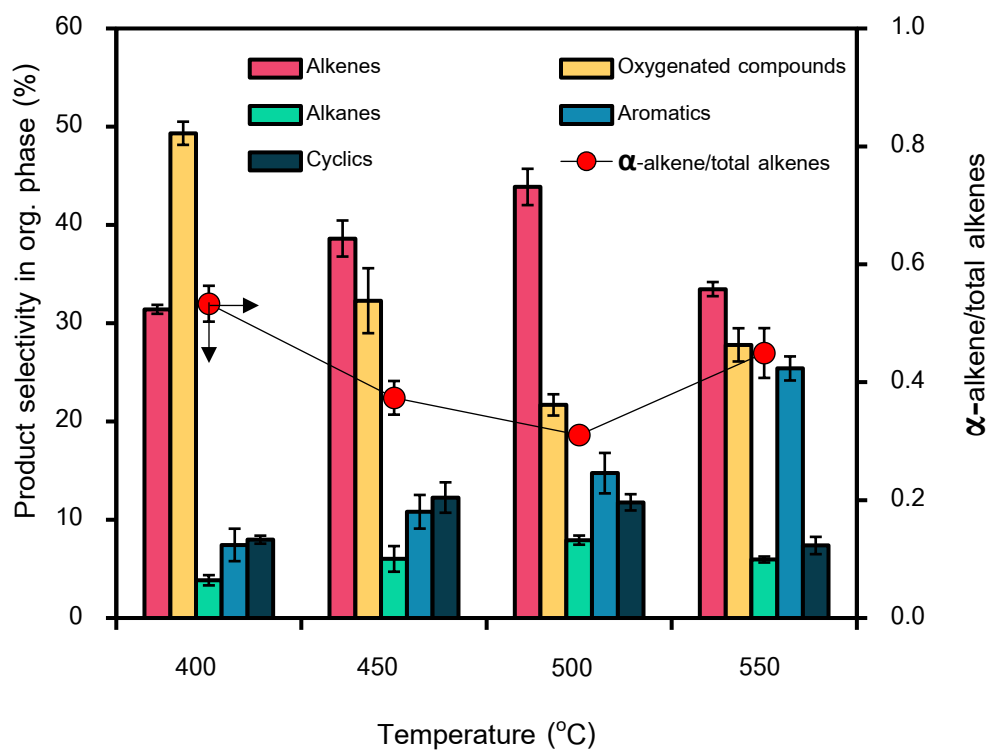
Figure 4.11 Effect of the reaction temperature on the selectivity in the organic phase of the liquid products and α-alkenes/total alkenes ratio obtained from ODH of OA using 1.0%V_xO_y/SBA-15 catalyst.
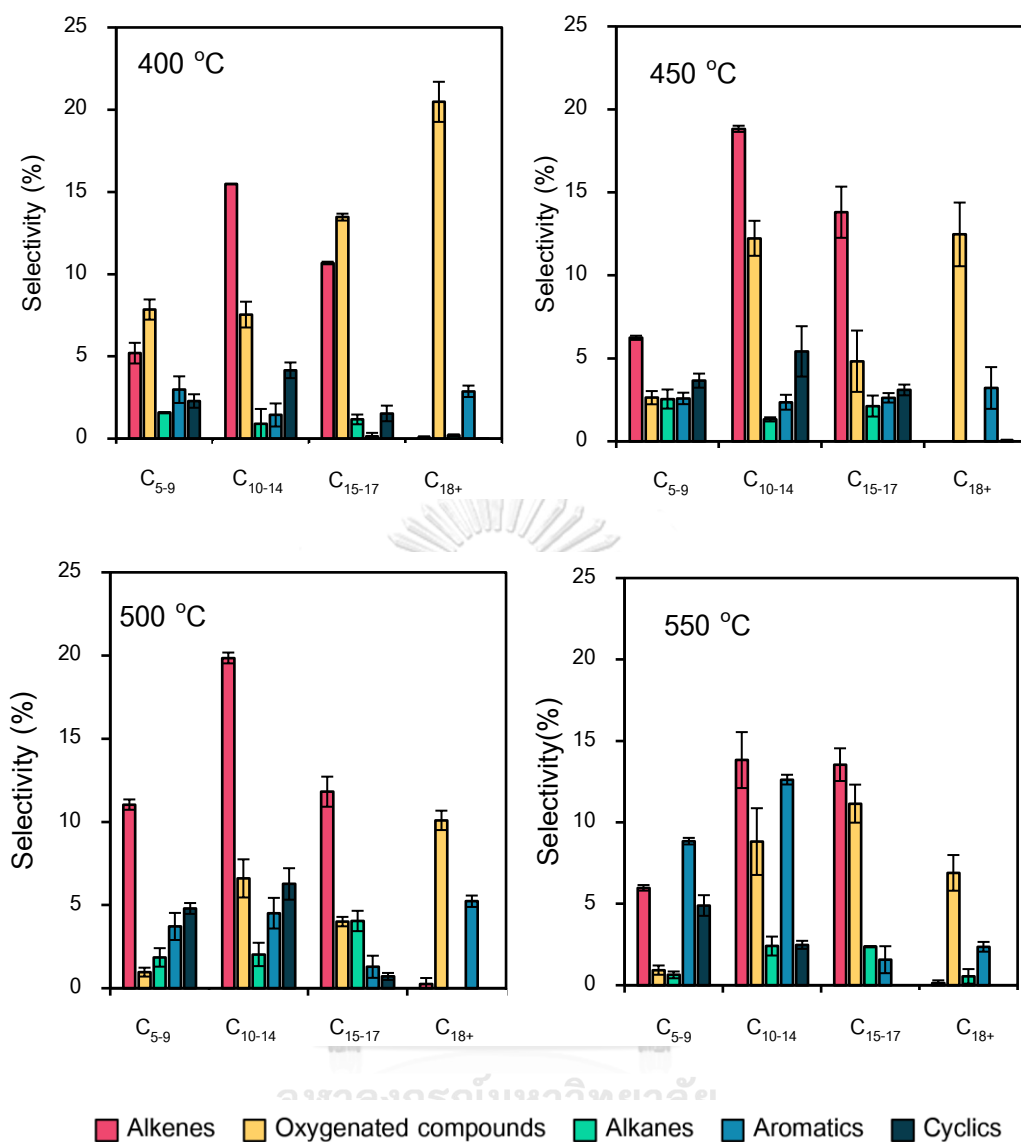
Figure 4.12 Effect of the reaction temperature on the distribution of carbon atoms in the organic phase of the liquid products obtained from ODH of using 1.0%V_xO_y/SBA-15 catalyst.
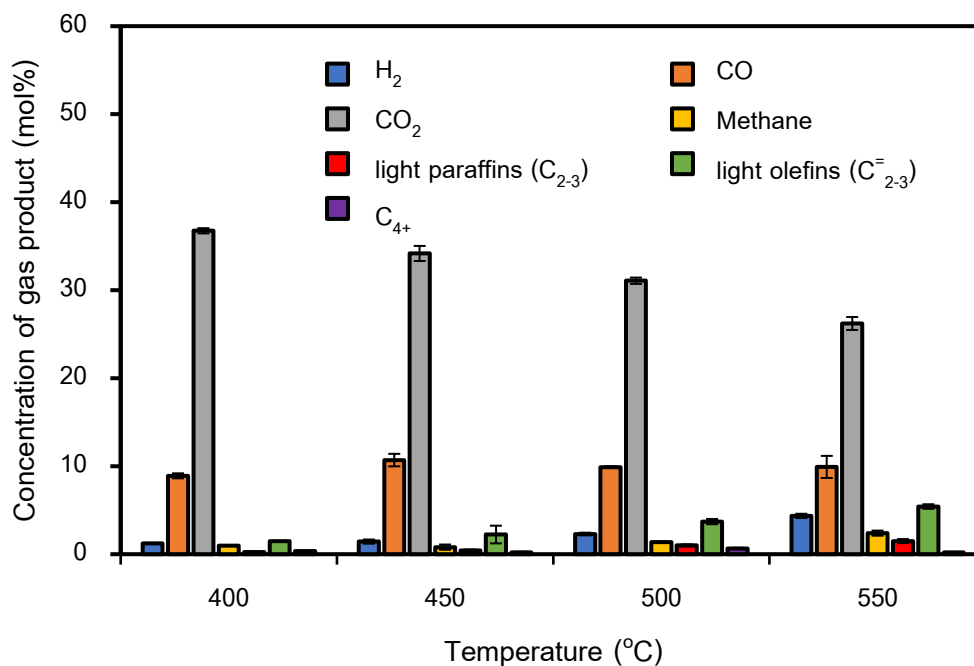
Figure 4.13 Effect of the reaction temperature on the concentration of gas products obtained from ODH of OA using $1.0\%V_xO_y$/SBA-15 catalyst.

3.2.3 Stability testing of 1.0% V_xO_y/SBA-15 catalyst

The catalyst stability testing for ODH of OA was performed over $1.0\%V_xO_y$/SBA-15 catalyst at 450 ^{o}C under 2, 6, and 8 h time on stream as shown in Figure 4.14. The performance to convert OA obviously decreased from 83.7% to 63.0% OA conversion when the time on stream was longer from 2 h to 8 h. Although the selectivity to alkenes had no significant change, the level of selectivity to oxygenated compounds slightly increased from 32.8% to 39.2%, with a decline in the aromatic selectivity. This implies that the catalyst's active site was changed. The analysis of SEM (Figure 4.15) shows the catalyst deactivation due to the collapse of its structure.
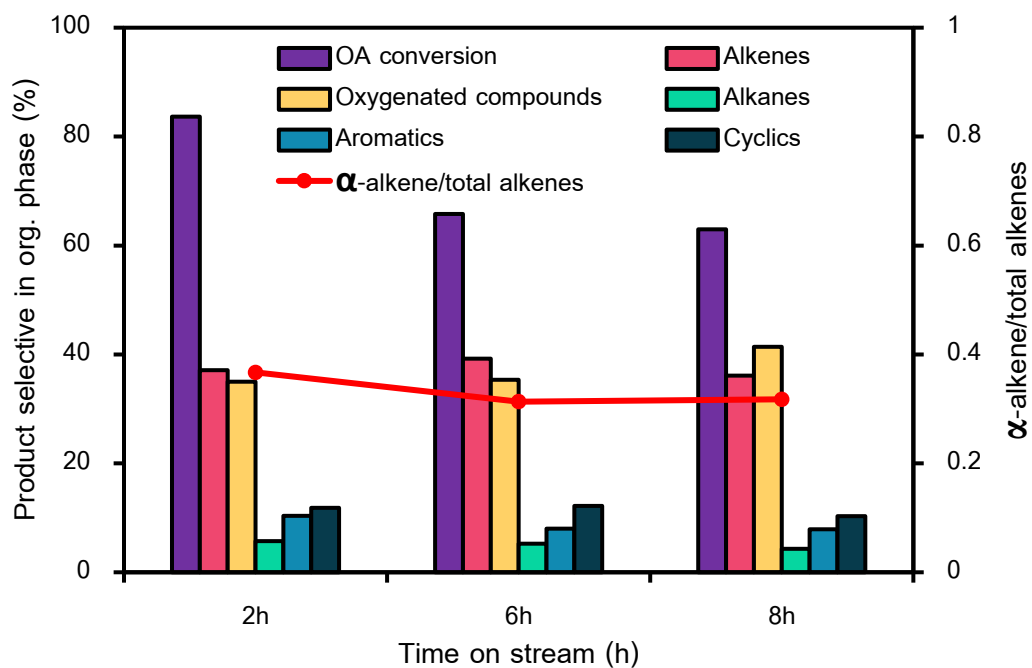
Figure 4.14 the stability testing of 1.0%V$_x$O$_y$/SBA-15 catalyst for ODH of OA in terms of the OA conversion and the product selectivity at each time on stream.
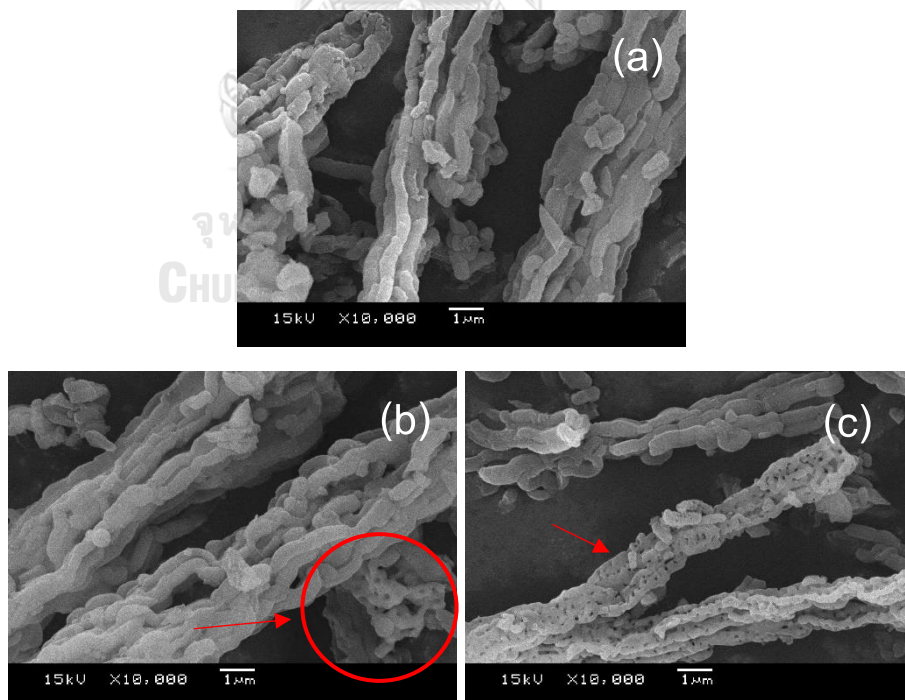
Figure 4.15 SEM images of spent 1.0%V$_x$O$_y$/SBA-15 catalyst: (a) 2 h, (b) 6 h, and (c) 8 h time on stream.

3.2.4 Regeneration and reusability of the 1.0% V_xO_y/SBA-15 catalyst

The reusability of 1.0% V_xO_y/SBA-15 catalyst was evaluated under the optimum reaction conditions at 450 $^{\circ}$C and 2 h time on stream. The spent catalyst obtained from each cycle was regenerated by calcining in the air at 600 $^{\circ}$C for 4 h. Figure 4.16 shows the performance of the spent catalyst and selectivity to species in the liquid products obtained from the ODH of OA. The OA conversion was dramatically decreased from 83.7% to 36.6% when the spent catalyst obtained from 3rd regeneration cycle was applied, whereas the selectivity to the oxygenated compounds increased from 35.0% to 59.4%. However, the selectivity to alkenes was slightly lowering. Although the SEM-EDX analysis (Figure 4.17) showed no significant change in the catalyst structure or vanadium agglomeration after the 3rd regeneration cycle, the TGA profiles between fresh and spent catalysts obtained from the 3rd regeneration cycle (Figure 4.18) obviously showed that the amount of coke deposited on the catalyst surface was dramatically increased from 1.8% to 9.0%. This suggests that the level of OA conversion was reduced due to the accumulation of coke, which reduced the active site of the catalyst.
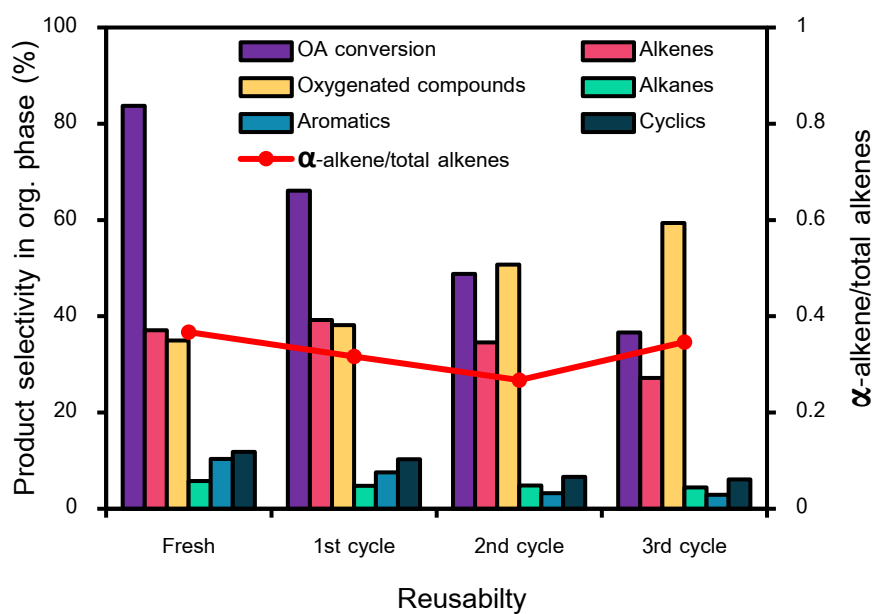
Figure 4.16 Effect of regeneration and reusability of the 1.0%V$_x$O$_y$/SBA-15 catalyst for the ODH of OA in terms of the OA conversion and the product selectivity at 450°C for 2 h time on stream.
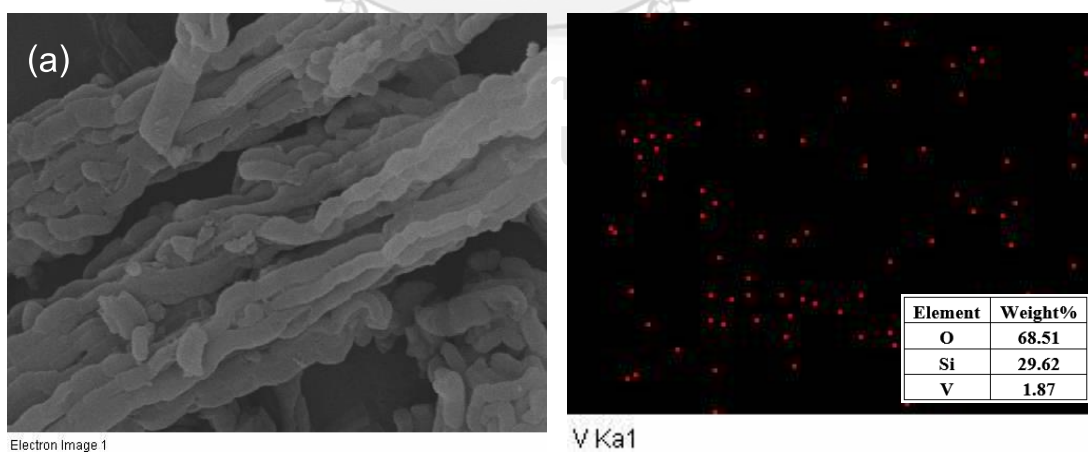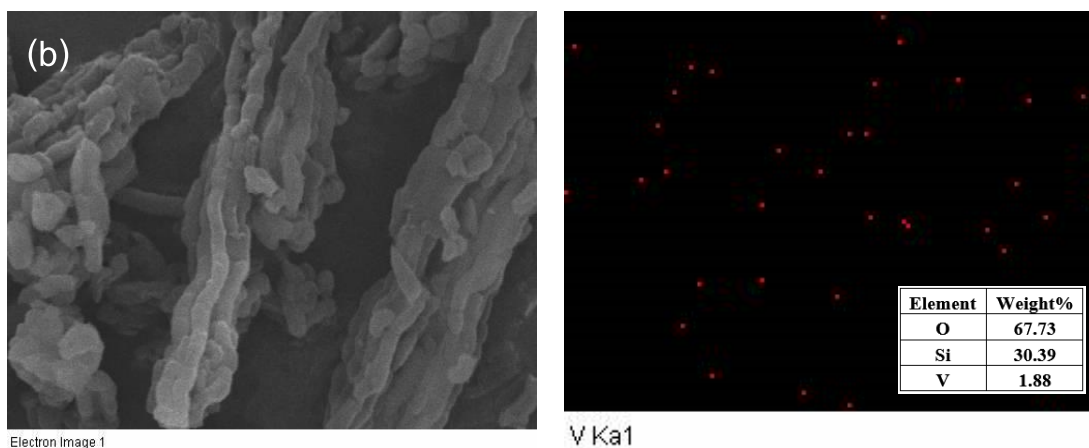
Figure 4.17 The SEM images of 1.0%V$_x$O$_y$/SBA-15 (a) fresh and (b) spent catalyst after the third cycle.
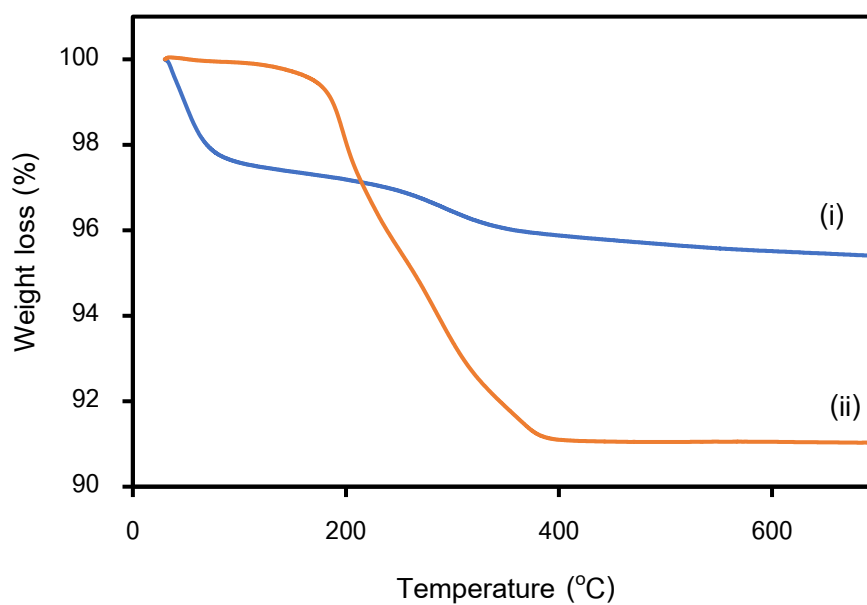
Figure 4.18 The TGA profile of the (i) fresh and (ii) spent 1.0%V$_x$O$_y$/SBA-15 catalysts obtained from ODH of OA at 450°C for 2 h time on stream.

CHAPTER V

CONCLUSION AND RECOMMENTATION

5.1 Conclusion

5.1.1 Catalyst characterization

The XRD analyses and HRTEM images confirmed the well-dispersed vanadium oxides on SBA-15. From the wide-angle XRD patterns, no diffraction peaks corresponding to V_2O_5 crystalline for nV_xO_y/SBA-15 catalysts were observed, while the HRTEM images clearly exhibited that the mesoporous structure of SBA-15 was preserved after loading the vanadium oxide. Moreover, the cluster or particle of V_xO_y was not appeared on the SBA-15 surface, although the high vanadium loading was applied. To confirm the presence of vanadium species in the prepared catalysts, the results of EDX mapping by TEM analysis of the nV_xO_y/SBA-15 catalysts showed the well-dispersed of vanadium species located in the internal pore of the catalysts, which was consistent with the results of the textural properties obtained from BET data. The high surface area and pore volume of SBA-15 decreased after the impregnation of vanadium content, suggesting that vanadium particles possibly blocked the pores of SBA-15. Whereas, there were no significant changes in the pore size. This indicated that the V_xO_y particles were deposited inside the pores of the SBA-15 support. The XPS data and H_2-TPR profiles revealed that the nV_xO_y/SBA-15 catalyst was consisted of two surface oxidation state, attributed to the V^{4+} in VO_2 and V^{5+} in V_2O_5 species. For the results obtained from the NH_3-TPD technique, the total acidity of catalyst increased with increasing the vanadium content. In particular, the intensity of weak acid desorption peaks dramatically increased and slightly shifted to the higher desorption temperature.

5.1.2 Effect of the different vanadium loading on ODH of OA

The V_xO_y/SBA-15 catalysts with different vanadium contents could convert oleic acid to produce bio-olefins via ODH reaction at 450 ^{o}C. The 1.0%V_xO_y/SBA-15 catalyst showed the highest oleic acid conversion at 83.7%, whereas 0.5%V_xO_y/SBA-15 catalyst provided the high selectivity to olefins with carbon atoms in the range of C_7-C_{17} (44.6%). The higher vanadium content to 3.0-5.0 wt% decreased the oleic acid conversion and selectivity to olefins due to reduced surface area and higher acidity of the catalysts that promoted the production of oxygenated compounds. Moreover, the α-alkenes/total alkenes ratio was highest at 0.58 when 3.0%V_xO_y/SBA-15 catalyst was applied because the catalysts with higher acidity could inhibit the desorption of the formed dienes from the catalyst surface, which were further formed as aromatics compounds. However, the use of the 5.0%V_xO_y/SBA-15 catalyst exhibited the dramatic reduction of α-alkenes/total alkenes ratio to 0.28 and the selectivity to aromatics was also decreased with the greater selectivity to oxygenated compounds. This was due to the overdose of vanadium species that could promote the deep oxidation.

5.1.3 Effect of temperature on ODH of OA

To consider the effect of temperature on ODH, it was observed that the increase in the reaction temperature from 400 ^{o}C to 450 ^{o}C increased the performance of catalyst to convert OA, whereas above this point (> 450 ^{o}C) the level of OA conversion tends to be slightly decreased due to the exothermic nature of the ODH reaction. Besides the OA conversion, the reaction temperature also affected the selectivity in the organic liquid phase. The increase in the reaction temperature to 500 ^{o}C provided the highest olefin selectivity (40.4%). At the same time, the increasing reaction temperature promoted the formation of aromatic compounds via thermal cracking of long-chain olefins to generate the alkyl benzenes. In addition, the contents of light hydrocarbons from thermal cracking increased when the reaction temperature

increased from 400 to 550 $^{\circ}$C. Whereas, the content of carbon dioxide decreased because the stability of the aromatic formation inhibited the secondary combustion.

5.1.4 Stability testing of 1.0% V_xO_y/SBA-15 catalyst

The catalyst stability testing for ODH of OA has been performed using the 1.0%V_xO_y/SBA-15 catalyst at 450 $^{\circ}$C under 2, 6, and 8 h time on stream. The results showed that the selectivity to alkenes had no significant change. The level of selectivity to oxygenated compounds slightly increased from 32.8% to 39.2%. However, the operation carried out longer than 2 h exhibited the catalyst deactivation due to the collapse of its structure.

5.1.5 Regeneration and reusability of the 1.0% V_xO_y/SBA-15 catalyst

To test the reusability of the catalyst, the 1.0% V_xO_y/SBA-15 catalyst was used to evaluate under the optimum reaction conditions at 450 $^{\circ}$C for 2 h time on stream. The result shows that the spent catalyst had a lower ability to convert OA due to the accumulation of coke, which reduced the active site of the catalyst.

5.2 Recommendation

- The nV_xO_y/SBA-15catalyst is sensitive to moisture. The change of its pristine color from yellow to green, indicates the deactivation of catalyst. Thus, the new catalyst having high resistance to moisture or water generated during ODH process should be further investigated.

-The direct use for palm olein as the raw materials for producing the long-chain bio-olefins should be studied to reduce the step of oleic acid separation.

- The process for separation and purification of the long-chain bio-olefins obtained from ODH process should be more studied for using as the raw materials for other applications.

REFERENCES

[1]   A. Zarli, "Oleochemicals: all time players of green chemistry," in *Catalysis, Green Chemistry and Sustainable Energy*, (Studies in Surface Science and Catalysis, 2020, pp. 77-95.

[2]   H. Cruchade *et al.*, "Cleaner technology for the production of linear long chain α-olefins through a "millisecond" oxidative cracking process," *Applied Catalysis A: General,* vol. 610, p. 117944, 2021/01/25/ 2021, doi: https://doi.org/10.1016/j.apcata.2020.117944.

[3]   W. Prasanseang, K. Choojun, Y. Poo-arporn, A.-L. Huang, Y.-C. Lin, and T. Sooknoi, "Linear long-chain α-olefins from hydrodeoxygenation of methyl palmitate over copper phyllosilicate catalysts," *Applied Catalysis A: General,* vol. 635, 2022, doi: 10.1016/j.apcata.2022.118555.

[4]   A. Chatterjee, S. H. Hopen Eliasson, and V. R. Jensen, "Selective production of linear α-olefins via catalytic deoxygenation of fatty acids and derivatives," *Catalysis Science & Technology,* 10.1039/C7CY02580G vol. 8, no. 6, pp. 1487-1499, 2018, doi: 10.1039/C7CY02580G.

[5]   M. Snåre, I. Kubičková, P. Mäki-Arvela, K. Eränen, and D. Y. Murzin, "Heterogeneous Catalytic Deoxygenation of Stearic Acid for Production of Biodiesel," *Industrial & Engineering Chemistry Research,* vol. 45, no. 16, pp. 5708-5715, 2006/08/01 2006, doi: 10.1021/ie060334i.

[6]   V. Yelchuri, K. Srikanth, R. B. N. Prasad, and M. S. L. Karuna, "Olefin metathesis of fatty acids and vegetable oils," *Journal of Chemical Sciences,* vol. 131, no. 5, 2019, doi: 10.1007/s12039-019-1615-8.

[7]   C. A. Gärtner, A. C. van Veen, and J. A. Lercher, "Oxidative Dehydrogenation of Ethane: Common Principles and Mechanistic Aspects," *ChemCatChem,* vol. 5, no. 11, pp. 3196-3217, 2013, doi: 10.1002/cctc.201200966.

[8]   B. Pillay, M. R. Mathebula, and H. B. Friedrich, "The oxidative dehydrogenation of n-hexane over Ni–Mo–O catalysts," *Applied Catalysis A: General,* vol. 361, no. 1-2,

pp. 57-64, 2009, doi: 10.1016/j.apcata.2009.03.032.

[9]   E. A. Elkhalifa and H. B. Friedrich, "Oxidative dehydrogenation of n-octane using vanadium-magnesium oxide catalysts with different vanadium loadings," *Applied Catalysis A: General,* vol. 373, no. 1-2, pp. 122-131, 2010, doi: 10.1016/j.apcata.2009.11.004.

[10]   V. D. B. C. Dasireddy, S. Singh, and H. B. Friedrich, "Vanadium oxide supported on non-stoichiometric strontium hydroxyapatite catalysts for the oxidative dehydrogenation of n-octane," *Journal of Molecular Catalysis A: Chemical,* vol. 395, pp. 398-408, 2014, doi: 10.1016/j.molcata.2014.08.044.

[11]   S. Najari *et al.*, "Oxidative dehydrogenation of ethane: catalytic and mechanistic aspects and future trends," *Chem Soc Rev,* vol. 50, no. 7, pp. 4564-4605, Apr 7 2021, doi: 10.1039/d0cs01518k.

[12]   G. Mitran *et al.*, "Propane oxidative dehydrogenation over VOx/SBA-15 catalysts," *Catalysis Today,* vol. 306, pp. 260-267, 2018, doi: 10.1016/j.cattod.2016.12.014.

[13]   W. Liu, S. Y. Lai, H. Dai, S. Wang, H. Sun, and C. T. Au, "Oxidative dehydrogenation of n-butane over mesoporous VOx/SBA-15 catalysts," *Catalysis Letters,* vol. 113, no. 3, pp. 147-154, 2007/02/01 2007, doi: 10.1007/s10562-007-9023-y.

[14]   D. Le, N. Chaidherasuwet, A. Rueangthaweep, C. Kulsing, and N. Hinchiranan, "Long-chain bio-olefins production via oxidative dehydrogenation of oleic acid over vanadium oxides/KIT-6 catalysts," *Catalysis Today,* 2021, doi: 10.1016/j.cattod.2021.07.034.

[15]   D. Le, N. Chaidherasuwet, and N. Hinchiranan, "Vanadium-magnesium oxides/KIT-6 catalysts for oxidative dehydrogenation of oleic acid to long-chain bio-olefins," *Applied Catalysis A: General,* vol. 638, 2022, doi: 10.1016/j.apcata.2022.118624.

[16]   B. Solsona, T. Blasco, J. M. López Nieto, M. L. Peña, F. Rey, and A. Vidal-Moya, "Vanadium Oxide Supported on Mesoporous MCM-41 as Selective Catalysts in the Oxidative Dehydrogenation of Alkanes," *Journal of Catalysis,* vol. 203, no. 2, pp. 443-452, 2001, doi: 10.1006/jcat.2001.3326.

[17]   A. Brückner, P. Rybarczyk, H. Kosslick, G. U. Wolf, and M. Baerns, "Highly

dispersed VOx species on mesoporous supports: Promising catalysts for the oxidative dehydrogenation (ODH) of propane," in *Studies in Surface Science and Catalysis*, vol. 142, R. Aiello, G. Giordano, and F. Testa Eds.: Elsevier, 2002, pp. 1141-1148.

[18] T. Blasco, J. M. L. Nieto, A. Dejoz, and M. I. Vazquez, "Influence of the Acid-Base Character of Supported Vanadium Catalysts on Their Catalytic Properties for the Oxidative Dehydrogenation of n-Butane," *Journal of Catalysis,* vol. 157, no. 2, pp. 271-282, 1995/12/01/ 1995, doi: https://doi.org/10.1006/jcat.1995.1291.

[19] V. Chaudhary and S. Sharma, "An overview of ordered mesoporous material SBA-15: synthesis, functionalization and application in oxidation reactions," *Journal of Porous Materials,* vol. 24, no. 3, pp. 741-749, 2017/06/01 2017, doi: 10.1007/s10934-016-0311-z.

[20] G. S. Mishra, K. Machado, and A. Kumar, "Highly selective n-alkanes oxidation to ketones with molecular oxygen catalyzed by SBA-15 supported rhenium catalysts," *Journal of Industrial and Engineering Chemistry,* vol. 20, no. 4, pp. 2228-2235, 2014, doi: 10.1016/j.jiec.2013.09.055.

[21] A. Wawrzyńczak, S. Jarmolińska, and I. Nowak, "Nanostructured KIT-6 materials functionalized with sulfonic groups for catalytic purposes," *Catalysis Today,* vol. 397-399, pp. 526-539, 2022, doi: 10.1016/j.cattod.2021.06.019.

[22] D. Santhanaraj, C. Suresh, A. Selvamani, and K. Shanthi, "A comparison study between V-SBA-15 and V-KIT-6 catalysts for selective oxidation of diphenylmethane," *New Journal of Chemistry,* vol. 43, no. 29, pp. 11554-11563, 2019, doi: 10.1039/c9nj02007a.

[23] W. Wang *et al.*, "Synthesis of KIT-6 type mesoporous silicas with tunable pore sizes, wall thickness and particle sizes via the partitioned cooperative self-assembly process," *Microporous and Mesoporous Materials,* vol. 194, pp. 167-173, 2014, doi: 10.1016/j.micromeso.2013.10.028.

[24] R. A. Ortega-Domínguez, H. Vargas-Villagrán, C. Peñaloza-Orta, K. Saavedra-Rubio, X. Bokhimi, and T. E. Klimova, "A facile method to increase metal dispersion

and hydrogenation activity of Ni/SBA-15 catalysts," *Fuel,* vol. 198, pp. 110-122, 2017, doi: 10.1016/j.fuel.2016.12.037.

[25]   A. de Reviere, D. Gunst, M. Sabbe, and A. Verberckmoes, "Sustainable short-chain olefin production through simultaneous dehydration of mixtures of 1-butanol and ethanol over HZSM-5 and γ-Al2O3," *Journal of Industrial and Engineering Chemistry,* vol. 89, pp. 257-272, 2020, doi: 10.1016/j.jiec.2020.05.022.

[26]   O. M. Basmage and M. S. J. Hashmi, "Plastic Products in Hospitals and Healthcare Systems," in *Encyclopedia of Renewable and Sustainable Materials*, 2020, pp. 648-657.

[27]   R. Le Van Mao, H. Yan, A. Muntasar, and N. Al-Yassir, "Blending of Non-Petroleum Compounds with Current Hydrocarbon Feeds to Use in the Thermo-Catalytic Steam-Cracking Process for the Selective Production of Light Olefins," in *New and Future Developments in Catalysis*, 2013, pp. 143-173.

[28]   S. F. Håkonsen and A. Holmen, "Oxidative Dehydrogenation of Alkanes," in *Handbook of Heterogeneous Catalysis*, pp. 3384-3400.

[29]   X. Wang and X. Lü, "More than biofuels," in *Advances in 2nd Generation of Bioethanol Production*, 2021, pp. 31-51.

[30]   H. Cruchade *et al.*, "Cleaner technology for the production of linear long chain α-olefins through a "millisecond" oxidative cracking process," *Applied Catalysis A: General,* vol. 610, 2021, doi: 10.1016/j.apcata.2020.117944.

[31]   M. Kayfeci, A. Keçebaş, and M. Bayat, "Hydrogen production," in *Solar Hydrogen Production*, 2019, pp. 45-83.

[32]   O. O. James, B. Chowdhury, M. A. Mesubi, and S. Maity, "Reflections on the chemistry of the Fischer–Tropsch synthesis," *RSC Advances,* vol. 2, no. 19, 2012, doi: 10.1039/c2ra20519j.

[33]   S. H. Kim and G. A. Somorjai, "Surface science of single-site heterogeneous olefin polymerization catalysts," *Proceedings of the National Academy of Sciences,* vol. 103, no. 42, pp. 15289-15294, 2006, doi: doi:10.1073/pnas.0602346103.

[34]   C. T. Young, R. von Goetze, A. K. Tomov, F. Zaccaria, and G. J. P. Britovsek, "The

Mathematics of Ethylene Oligomerisation and Polymerisation," *Topics in Catalysis,* vol. 63, no. 3-4, pp. 294-318, 2020, doi: 10.1007/s11244-019-01210-0.

[35] B. Yilmaz and D. Agagunduz, "Fractionated palm oils: emerging roles in the food industry and possible cardiovascular effects," *Crit Rev Food Sci Nutr,* vol. 62, no. 7, pp. 1990-1998, 2022, doi: 10.1080/10408398.2020.1869694.

[36] A. Rabiu, S. Elias, and O. Oyekola, "Oleochemicals from Palm Oil for the Petroleum Industry," in *Palm Oil*, 2018, ch. Chapter 6.

[37] M. E. Norhaizan, S. Hosseini, S. Gangadaran, S. T. Lee, F. R. Kapourchali, and M. H. Moghadasian, "Palm oil: Features and applications," *Lipid Technology,* vol. 25, no. 2, pp. 39-42, 2013, doi: 10.1002/lite.201300254.

[38] K. Sakai, M. A. Hassan, C. S. Vairappan, and Y. Shirai, "Promotion of a green economy with the palm oil industry for biodiversity conservation: A touchstone toward a sustainable bioindustry," *J Biosci Bioeng,* vol. 133, no. 5, pp. 414-424, May 2022, doi: 10.1016/j.jbiosc.2022.01.001.

[39] K. Fukudome, N.-o. Ikenaga, T. Miyake, and T. Suzuki, "Oxidative dehydrogenation of propane using lattice oxygen of vanadium oxides on silica," *Catalysis Science & Technology,* vol. 1, no. 6, 2011, doi: 10.1039/c1cy00115a.

[40] S. V. Sancheti, G. D. Yadav, and P. K. Ghosh, "Synthesis and Application of Novel NiMoK/TS-1 for Selective Conversion of Fatty Acid Methyl Esters/Triglycerides to Olefins," *ACS Omega,* vol. 5, no. 10, pp. 5061-5071, 2020/03/17 2020, doi: 10.1021/acsomega.9b03993.

[41] N. Krobkrong, V. Itthibenchapong, P. Khongpracha, and K. Faungnawakij, "Deoxygenation of oleic acid under an inert atmosphere using molybdenum oxide-based catalysts," *Energy Conversion and Management,* vol. 167, pp. 1-8, 2018, doi: 10.1016/j.enconman.2018.04.079.

[42] A. Chatterjee and V. R. Jensen, "A Heterogeneous Catalyst for the Transformation of Fatty Acids to α-Olefins," *ACS Catalysis,* vol. 7, no. 4, pp. 2543-2547, 2017, doi: 10.1021/acscatal.6b03460.

[43] Y.-M. Liu *et al*., "Vanadium oxide supported on mesoporous SBA-15 as highly

selective catalysts in the oxidative dehydrogenation of propane," *Journal of Catalysis,* vol. 224, no. 2, pp. 417-428, 2004, doi: 10.1016/j.jcat.2004.03.010.

[44]   C. Wei *et al*., "Dehydrogenation of Isobutane with Carbon Dioxide over SBA-15-Supported Vanadium Oxide Catalysts," *Catalysts,* vol. 6, no. 11, 2016, doi: 10.3390/catal6110171.

[45]   H. Atashin and R. Malakooti, "Supported Palladium Oxide Nanoparticles in SBA-15 as a Heterogeneous Catalyst for the Aerobic Oxidation of Alcohols," *Journal of the Chinese Chemical Society,* vol. 61, no. 9, pp. 1039-1044, 2014, doi: 10.1002/jccs.201300609.

[46]   N. O. Ramoraswi and P. G. Ndungu, "Photo-Catalytic Properties of TiO2 Supported on MWCNTs, SBA-15 and Silica-Coated MWCNTs Nanocomposites," *Nanoscale Research Letters,* vol. 10, no. 1, p. 427, 2015/10/30 2015, doi: 10.1186/s11671-015-1137-3.

[47]   L. Y. Jaramillo, W. Henao, and M. Romero-Sáez, "Synthesis and characterization of MCM-41–SBA-15 mixed-phase silica with trimodal mesoporous system and thick pore wall," *Journal of Porous Materials,* vol. 27, no. 6, pp. 1669-1676, 2020, doi: 10.1007/s10934-020-00930-z.

[48]   R. Zhang, D. Shi, N. Liu, Y. Cao, and B. Chen, "Mesoporous SBA-15 promoted by 3d-transition and noble metals for catalytic combustion of acetonitrile," *Applied Catalysis B: Environmental,* vol. 146, pp. 79-93, 2014, doi: 10.1016/j.apcatb.2013.03.028.

[49]   C. Autthanit, P. Praserthdam, and B. Jongsomjit, "Oxidative and non-oxidative dehydrogenation of ethanol to acetaldehyde over different VOx/SBA-15 catalysts," *Journal of Environmental Chemical Engineering,* vol. 6, no. 5, pp. 6516-6529, 2018, doi: 10.1016/j.jece.2018.10.015.

[50]   S. Rayati, P. Nafarieh, and M. M. Amini, "The synthesis, characterization and catalytic application of manganese porphyrins bonded to novel modified SBA-15," *New Journal of Chemistry,* vol. 42, no. 8, pp. 6464-6471, 2018, doi: 10.1039/c8nj00743h.

—

[51]   H. Zhang, M. Li, P. Xiao, D. Liu, and C. J. Zou, "Structure and Catalytic Performance of Mg-SBA-15-Supported Nickel Catalysts for CO2Reforming of Methane to Syngas," *Chemical Engineering & Technology,* pp. n/a-n/a, 2013, doi: 10.1002/ceat.201300006.

[52]   E. Hryha, E. Rutqvist, and L. Nyborg, "Stoichiometric vanadium oxides studied by XPS," *Surface and Interface Analysis,* vol. 44, no. 8, pp. 1022-1025, 2012, doi: 10.1002/sia.3844.

[53]   M. Prześniak-Welenc, J. Karczewski, J. Smalc-Koziorowska, M. Łapiński, W. Sadowski, and B. Kościelska, "The influence of nanostructure size on V2O5 electrochemical properties as cathode materials for lithium ion batteries," *RSC Advances,* 10.1039/C6RA05695D vol. 6, no. 61, pp. 55689-55697, 2016, doi: 10.1039/C6RA05695D.

[54]   H. Wang, X. Huang, B. Li, and J. Gao, "Facile preparation of super-hydrophobic nanofibrous membrane for oil/water separation in a harsh environment," *Journal of Materials Science,* vol. 53, no. 14, pp. 10111-10121, 2018, doi: 10.1007/s10853-018-2312-6.

[55]   C. Wang *et al.,* "One-pot extraction and aerobic oxidative desulfurization with highly dispersed V2O5/SBA-15 catalyst in ionic liquids," *RSC Advances,* vol. 7, no. 62, pp. 39383-39390, 2017, doi: 10.1039/c7ra07286d.

[56]   C. Deng *et al.,* "The effect of positioning cations on acidity and stability of the framework structure of Y zeolite," *Sci Rep,* vol. 6, p. 23382, Mar 18 2016, doi: 10.1038/srep23382.

[57]   X.-L. Xue, W.-Z. Lang, X. Yan, and Y.-J. Guo, "Dispersed Vanadium in Three-Dimensional Dendritic Mesoporous Silica Nanospheres: Active and Stable Catalysts for the Oxidative Dehydrogenation of Propane in the Presence of CO2," *ACS Applied Materials & Interfaces,* vol. 9, no. 18, pp. 15408-15423, 2017, doi: 10.1021/acsami.7b01498.

[58]   D. Jiraroj, O. Jirarattanapochai, W. Anutrasakda, J. S. M. Samec, and D. N. Tungasmita, "Selective decarboxylation of biobased fatty acids using a Ni-FSM-16

catalyst," *Applied Catalysis B: Environmental,* vol. 291, 2021, doi: 10.1016/j.apcatb.2021.120050.

[59] Z. D. Yigezu and K. Muthukumar, "Biofuel production by catalytic cracking of sunflower oil using vanadium pentoxide," *Journal of Analytical and Applied Pyrolysis,* vol. 112, pp. 341-347, 2015, doi: 10.1016/j.jaap.2015.01.002.

[60] T. Garcia, B. Solsona, D. Murphy, K. Antcliff, and S. Taylor, "Deep oxidation of light alkanes over titania-supported palladium/vanadium catalysts," *Journal of Catalysis,* vol. 229, no. 1, pp. 1-11, 2005, doi: 10.1016/j.jcat.2004.09.018.

[61] M. F. Kamaruzaman, Y. H. Taufiq-Yap, and D. Derawi, "Green diesel production from palm fatty acid distillate over SBA-15-supported nickel, cobalt, and nickel/cobalt catalysts," *Biomass and Bioenergy,* vol. 134, 2020, doi: 10.1016/j.biombioe.2020.105476.

[62] J. P. Lourenço, M. I. Macedo, and A. Fernandes, "Sulfonic-functionalized SBA-15 as an active catalyst for the gas-phase dehydration of Glycerol," *Catalysis Communications,* vol. 19, pp. 105-109, 2012, doi: 10.1016/j.catcom.2011.12.029.

[63] Y. W. Cheng, C. C. Chong, C. K. Cheng, K. H. Ng, T. Witoon, and J. C. Juan, "Ethylene production from ethanol dehydration over mesoporous SBA-15 catalyst derived from palm oil clinker waste," *Journal of Cleaner Production,* vol. 249, 2020, doi: 10.1016/j.jclepro.2019.119323.

[64] M. Engeser, D. Schröder, and H. Schwarz, "Dehydration and Dehydrogenation of Alcohols with Mononuclear Cationic Vanadium Oxides in the Gas Phase and Energetics of VO

n

H

0/+

(

n

= 2, 3)," *European Journal of Inorganic Chemistry,* vol. 2007, no. 17, pp. 2454-2464, 2007, doi: 10.1002/ejic.200700062.

[65]   W. W. Christie and G. Dobson, "Formation of cyclic fatty acids during the frying process," *European Journal of Lipid Science and Technology,* vol. 102, no. 8-9, pp. 515-520, 2000, doi: https://doi.org/10.1002/1438-9312(200009)102:8/9<515::AID-EJLT515>3.0.CO;2-Z.

[66]   F. Destaillats and P. Angers, "On the mechanisms of cyclic and bicyclic fatty acid monomer formation in heated edible oils," *European Journal of Lipid Science and Technology,* vol. 107, no. 10, pp. 767-772, 2005, doi: 10.1002/ejlt.200501159.

[67]   E. A. Elkhalifa and H. B. Friedrich, "Oxidative dehydrogenation and aromatization of n-octane over VMgO catalysts obtained by using different MgO precursors and different precursor treatments," *Journal of Molecular Catalysis A: Chemical,* vol. 392, pp. 22-30, 2014, doi: 10.1016/j.molcata.2014.04.018.

[68]   F. van der Klis, J. Le Nôtre, R. Blaauw, J. van Haveren, and D. S. van Es, "Renewable linear alpha olefins by selective ethenolysis of decarboxylated unsaturated fatty acids," *European Journal of Lipid Science and Technology,* vol. 114, no. 8, pp. 911-918, 2012, doi: 10.1002/ejlt.201200024.

[69]   S. Singh, A. Bhadani, and B. Singh, "Synthesis of Wax Esters from α-Olefins," *Industrial & Engineering Chemistry Research,* vol. 46, no. 8, pp. 2672-2676, 2007/04/01 2007, doi: 10.1021/ie0616592.

[70]   V. D. B. C. Dasireddy, S. Singh, and H. B. Friedrich, "Oxidative dehydrogenation of n-octane using vanadium pentoxide-supported hydroxyapatite catalysts," *Applied Catalysis A: General,* vol. 421-422, pp. 58-69, 2012, doi: 10.1016/j.apcata.2012.01.034.

[71]   F. Li *et al.*, "Production of Light Olefins from Catalytic Cracking Bio-oil Model Compounds over La2O3-Modified ZSM-5 Zeolite," *Energy & Fuels,* vol. 32, no. 5, pp. 5910-5922, 2018, doi: 10.1021/acs.energyfuels.7b04150.

[72]   S. Sartipi, M. Makkee, F. Kapteijn, and J. Gascon, "Catalysis engineering of

bifunctional solids for the one-step synthesis of liquid fuels from syngas: a review," *Catal. Sci. Technol.,* vol. 4, no. 4, pp. 893-907, 2014, doi: 10.1039/c3cy01021j.

[73]   G. Noh, Z. Shi, S. I. Zones, and E. Iglesia, "Isomerization and β-scission reactions of alkanes on bifunctional metal-acid catalysts: Consequences of confinement and diffusional constraints on reactivity and selectivity," *Journal of Catalysis,* vol. 368, pp. 389-410, 2018, doi: 10.1016/j.jcat.2018.03.033.

[74]   A. But, J. Le Notre, E. L. Scott, R. Wever, and J. P. Sanders, "Selective oxidative decarboxylation of amino acids to produce industrially relevant nitriles by vanadium chloroperoxidase," *ChemSusChem,* vol. 5, no. 7, pp. 1199-202, Jul 2012, doi: 10.1002/cssc.201200098.

[75]   Z. Zhou, H. Liu, Z. Chen, W. Zhu, and Z. Liu, "Decarbonylation of Carboxylic Acids over H-Mordenite," *ACS Catalysis,* vol. 11, no. 7, pp. 4077-4083, 2021, doi: 10.1021/acscatal.1c00235.

[76]   A. S. Ello, A. Enferadi-kerenkan, A. Trokourey, and T.-O. Do, "Sustainable Oxidative Cleavage of Vegetable Oils into Diacids by Organo-Modified Molybdenum Oxide Heterogeneous Catalysts," *Journal of the American Oil Chemists' Society,* vol. 94, no. 12, pp. 1451-1461, 2017, doi: 10.1007/s11746-017-3047-2.

[77]   V. Benessere *et al.*, "Sustainable Process for Production of Azelaic Acid Through Oxidative Cleavage of Oleic Acid," *Journal of the American Oil Chemists' Society,* vol. 92, no. 11-12, pp. 1701-1707, 2015, doi: 10.1007/s11746-015-2727-z.

[78]   A. Enferadi Kerenkan, F. Béland, and T.-O. Do, "Chemically catalyzed oxidative cleavage of unsaturated fatty acids and their derivatives into valuable products for industrial applications: a review and perspective," *Catalysis Science & Technology,* vol. 6, no. 4, pp. 971-987, 2016, doi: 10.1039/c5cy01118c.

[79]   Z. Huang *et al.*, "Oxidative Cleavage of Alkenes by O2 with a Non-Heme Manganese Catalyst," *J Am Chem Soc,* vol. 143, no. 26, pp. 10005-10013, Jul 7 2021, doi: 10.1021/jacs.1c05757.

[80]   A. Ishihara, Y. Tsuchimori, and T. Hashimoto, "Dehydrocyclization-cracking of methyl oleate by Pt catalysts supported on a ZnZSM-5-Al2O3 hierarchical

composite," *RSC Adv,* vol. 11, no. 32, pp. 19864-19873, May 27 2021, doi: 10.1039/d1ra02677a.

จุฬาลงกรณ์มหาวิทยาลัย
CHULALONGKORN UNIVERSITY

APPENDIX A

CALCULATION OF CATALYST PREPARATION

The nV_xO_y/SBA-15 catalysts were preparation by wet impregnation method with different vanadium content on SBA-15 including 0.5, 1.0, 3.0, and 5.0 wt%. The calculation of preparation are shows as follow;

0.5%V_xO_y/SBA-15;   SBA-15 100 g has V 0.5 g

$$\text{SBA-15 1 g has V} = \frac{0.5}{100} = 0.005 \text{ g}$$

1.0%V_xO_y/SBA-15;   SBA-15 100 g has V 1.0 g

$$\text{SBA-15 1 g has V} = \frac{1.0}{100} = 0.01 \text{ g}$$

3.0%V_xO_y/SBA-15;   SBA-15 100 g has V 3.0 g

$$\text{SBA-15 1 g has V} = \frac{3.0}{100} = 0.03 \text{ g}$$

5.0%V_xO_y/SBA-15;   SBA-15 100 g has V 5.0 g

$$\text{SBA-15 1 g has V} = \frac{5.0}{100} = 0.05 \text{ g}$$

With V solution prepared by NH_4VO_3 (precursor) which has molecular weight = 116.98 g/mol and V has molecular weight = 50.94 g/mol

There is V 50.94 g/mol of NH_4VO_3 = 116.98 g/mol

So, V 0.005 g uses $NH_4VO_3 = \dfrac{0.005 \times 116.98}{50.94} = 0.0115$ g of NH_4VO_3 reagent.

APPENDIX B

CALCULATION

1. The conversion of oleic acid was calculated by standard curve of oleic acid.

$$\%\text{Conversion} = 100 - \%\text{OA(unreaction)}$$

$$\%\text{OA (unreaction)} = \frac{(\text{peak area of OA unreaction})}{\text{peak area of OA}} \times 100$$

2. Product distribution calculation after ODH reaction

    2.1 Liquid product

$$\text{Liquid product with OA (g)} = \text{condensation flask after (g)} - \text{condensation flask before (g)}$$

$$\text{OA (unreaction)(g)} = \frac{(\text{OA feed})(\text{g}) \times (100 - \%\text{conversion})}{100}$$

$$\text{Liquid product from OA (g)} = \text{liquid product with OA (g)} - \text{OA feed (g)}$$

    2.2 Solid product

$$\text{Solid product (g)} = \frac{\text{solid TGA (\%)} \times \text{catalyst feed (g)}}{100 - \text{solid TGA (\%)}}$$

    2.3 Gas product

$$\text{Gas product (g)} = \text{OA feed(g)} - \text{OA unreaction (g)} - \text{liquid product(g)} - \text{solid product(g)}$$

3. Selectivity (S_i) calculation in liquid and gas products

3.1 Liquid product

$$\%\text{Selectivity} = \frac{\text{peak area}}{\text{total area}} \times 100$$

when "total area" was the summation of the peak area of the compositions found in the liquid product obtained from GC-MS data except the peak area of OA.

3.2 Gas product

$$\text{Concentration of gas (\%mol)} = \frac{\text{peak area of product} \times \text{standgard gas (\%mol)}}{\text{peak area of standard gas}}$$

when "peak area" was found in the liquid product obtained from GC-FID and GC-TCD data.

For example, using the 1.0%V_xO_y/SBA-15 catalyst of ODH reaction.

Table B1 Data weight of oleic acid, catalyst, glass bead, condensation flask of ODH reaction

ODH of OA using 1.0%V_xO_y/SBA-15 catalyst	
Weight of catalyst	0.2053 g
Weight of glass bead	2.0094 g
Weight of oleic acid	10.4587 g
Weight of condensation flask	806.58 g
Weight of condensation flask after	814.94 g
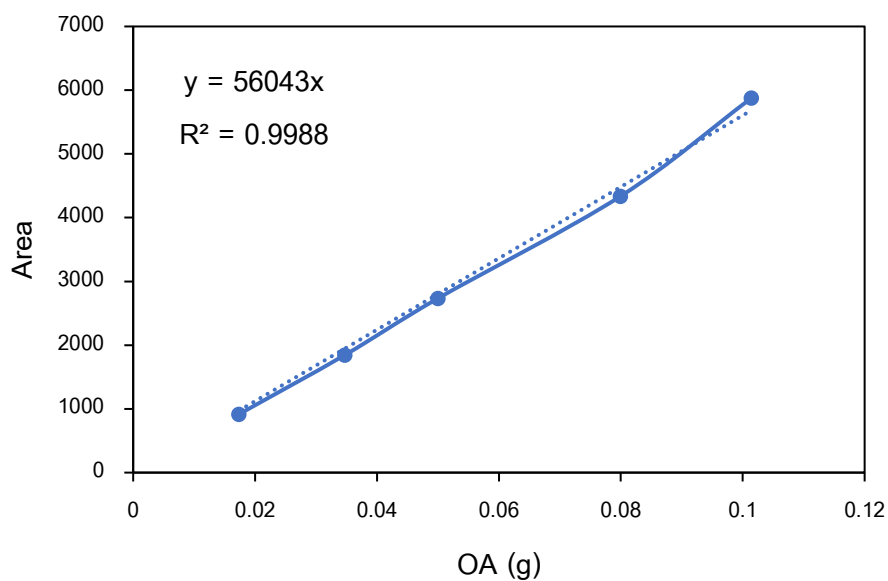
Figure B1 Standard curve of OA.

-The conversion of oleic acid was calculated by standard curve of oleic acid.

$$\%OA \ (unreaction) = \frac{796.3}{5694.0} \times 100 = 13.98$$

$$\%Conversion = 100 - 13.98 \ = 86.02$$

-Product distribution calculation after ODH reaction

Liquid products;

$$Liquid \ product \ with \ OA \ (g) = 814.94 - 806.58 = 8.36 \ g$$

$$OA \ (unreaction)(g) = \frac{10.4587 \ \times 13.98}{100} = 1.46 \ g$$

$$Liquid \ product \ from \ OA \ (g) = 8.36 - 1.46 \ = 6.90 \ g$$

Solid products;

$$Solid \ product \ (g) = \frac{1.8418 \times 0.2053}{100 - 1.8418} = 0.0040 \ g$$

Gas products;

$$Gas \ product \ (g) = 10.4587 - 1.46 - 6.90 - 0.0040 = 2.09 \ g$$

Table B2 Calculation of composition in liquid product obtained from GC-MS data

Composition in liquid products	Peak area
Alkanes	9187274
Alkenes	52872469
Aromatics	15922831
Oxygenated compounds	14791320
Cyclics	39677717
Total	132451611

Table B3 Calculation of composition in gas product obtained from GC-FID and GC-TCD data

Composition in gas products	Peak area of product	Peak area of STD. gas	Volume of STD. gas
H_2	29557.4	144568.9	5
CO	53375.5	17232.95	10
CO_2	61408.8	20715.1	10
CH_4	18099212	187270296	4.99
C_2H_4	67836078	350917878	5.01
C_2H_6	15254336	368573431	5.03
C_3H_6	29730263	534401900	4.99
C_3H_8	11576847	565091332	5
C_3H_4	304059	508445754	5.08
C_4	20817687	3351459258	5
C_{4+}	16355984	936351480	4.99

-Selectivity (S_i) calculation in liquid and gas products

Liquid product;

$$\%\text{Selectivity of alkenes} = \frac{52872469}{132451611} \times 100 = 40\%$$

Gas product;

$$\text{Concentration of methtane (\%mol)} = \frac{18099212 \times 4.99}{187270296} = 0.48\%\text{mol}$$
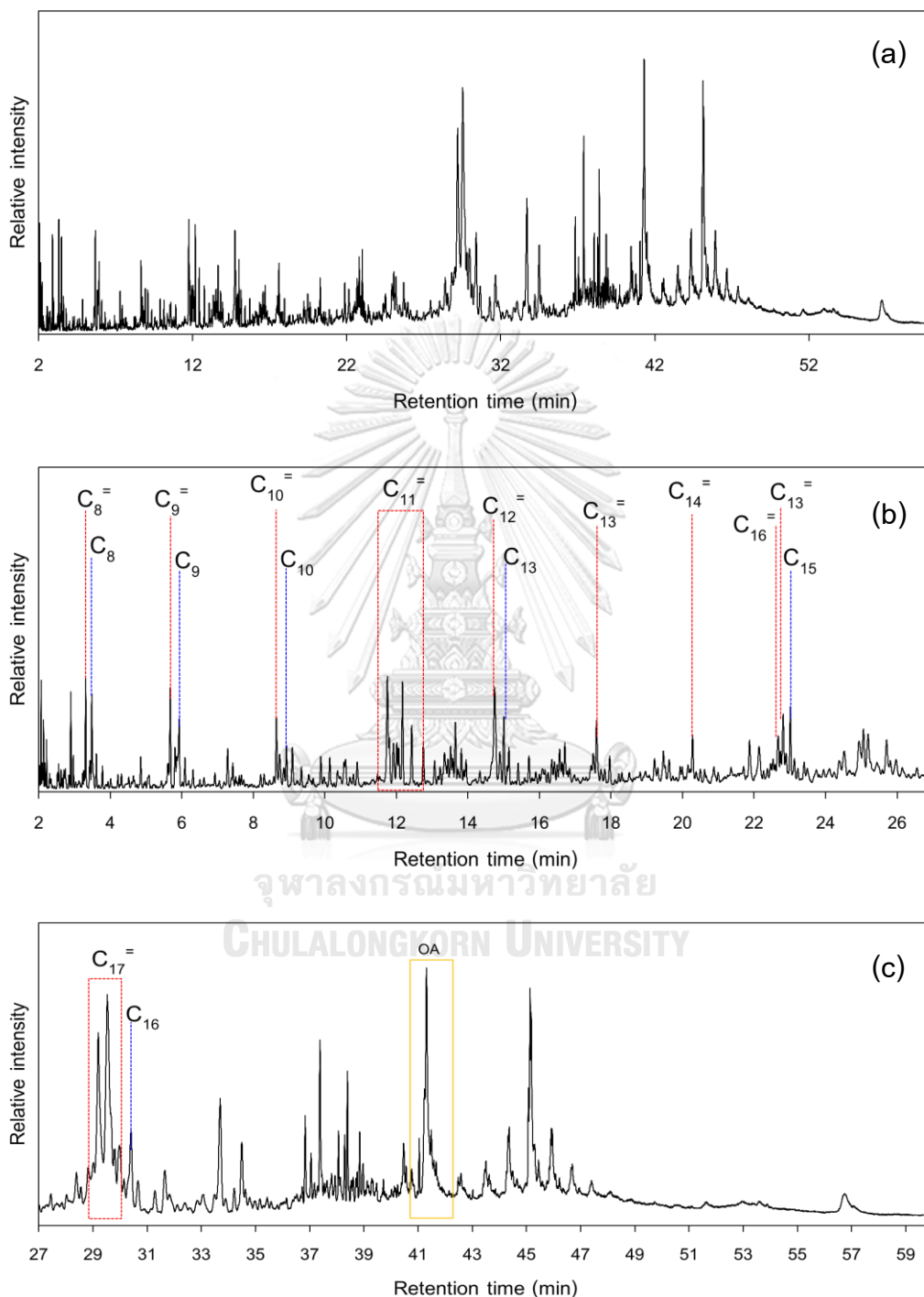
APPENDIX C

EXPIREMENTAL DATA

Figure C1 GC-MS chromatograms of liquid product at (a) overall retention time, (b) retention time 2-27 min, and (c) retention time 27-60 min from 1.0%V_xO_y/SBA-15 catalyst.

Table C1 GC-FID and GC-TCD data obtained from ODH of OA

Catalyst	Temp. (°C)	Concentration of gas product (%mol)						
		H_2	CO	CO_2	Methane	light paraffins (C2-C3)	light olefins (C2-C3)	C4+
SBA-15	450	1.09 ± 0.02	13.26 ± 0.34	31.15 ± 0.56	0.79 ± 0.03	0.48 ± 0.02	2.67 ± 0.14	0.55 ± 0.01
0.5%V_xO_y/SBA-15	450	1.07 ± 0.64	12.28 ± 0.62	30.06 ± 0.26	0.94 ± 0.03	0.71 ± 0.06	4.04 ± 0.45	0.90 ± 0.18
1.0%V_xO_y/SBA-15	450	1.43 ± 0.24	10.70 ± 0.71	34.17 ± 0.86	0.80 ± 0.03	0.44 ± 0.09	2.24 ± 1.00	0.22 ± 0.06
3.0%V_xO_y/SBA-15	450	2.62 ± 1.33	7.65 ± 0.29	35.60 ± 1.78	1.01 ± 0.01	0.56 ± 0.08	2.15 ± 0.29	0.41 ± 0.06
5.0%V_xO_y/SBA-15	450	8.46 ± 0.30	14.21 ± 0.60	26.60 ± 0.52	1.19 ± 0.05	0.74 ± 0.18	2.83 ± 0.27	0.21 ± 0.26
1.0%V_xO_y/SBA-15	400	0.79 ± 0.04	6.85 ± 0.31	25.52 ± 0.15	0.79 ± 0.00	0.21 ± 0.00	1.19 ± 0.01	0.30 ± 0.00
1.0%V_xO_y/SBA-15	500	1.39 ± 0.18	7.40 ± 0.22	20.31 ± 1.50	1.45 ± 0.07	1.06 ± 0.01	3.94 ± 0.09	0.70 ± 0.16
1.0%V_xO_y/SBA-15	550	2.53 ± 0.09	7.21 ± 0.58	16.49 ± 0.68	2.23 ± 0.25	1.39 ± 0.20	5.04 ± 0.20	0.19 ± 0.02

Table C2 GC-MS data obtained from ODH of OA with various vanadium contents

Catalyst	Product selectivity in org. phase (%)						α-alkene/total alkenes
	Alkanes	Alkenes	Aromatics	Cyclics	Oxygenates compounds		
SBA-15	3.59 ± 0.24	43.20 ± 1.57	3.54 ± 0.12	9.35 ± 0.20	40.33 ± 1.73		0.26 ± 0.00
0.5%V_xO_y/SBA-15	5.46 ± 0.54	44.64 ± 1.39	8.36 ± 0.94	12.79 ± 0.10	28.75 ± 0.89		0.24 ± 0.00
1.0%V_xO_y/SBA-15	6.01 ± 1.30	38.62 ± 1.84	10.81 ± 1.71	12.26 ± 1.55	32.29 ± 3.31		0.37 ± 0.03
3.0%V_xO_y/SBA-15	7.19 ± 0.84	31.91 ± 0.67	13.92 ± 1.85	10.18 ± 1.16	36.80 ± 2.20		0.58 ± 0.03
5.0%V_xO_y/SBA-15	6.38 ± 1.20	33.47 ± 1.20	8.55 ± 1.98	7.31 ± 0.69	44.28 ± 0.30		0.28 ± 0.01

Table C3 GC-MS data obtained from ODH of OA using 1.0%V_xO_y/SBA-15 catalyst with various reaction temperature

Temperature (°C)	Product selectivity in org. phase (%)					α-alkene/total alkenes
	Alkanes	Alkenes	Aromatics	Cyclics	Oxygenates compounds	
400	3.84 ± 0.52	31.42 ± 0.46	7.44 ± 1.65	7.97 ± 0.41	49.33 ± 1.18	0.53 ± 0.03
500	7.93 ± 0.47	43.87 ± 1.85	14.74 ± 2.06	11.77 ± 0.83	21.69 ± 1.08	0.31 ± 0.01
550	5.95 ± 0.31	33.47 ± 0.72	25.40 ± 1.23	7.38 ± 0.88	27.80 ± 1.69	0.45 ± 0.04

Table C4 GC-MS data obtained from ODH of OA using 1.0%V_xO_y/SBA-15 catalyst with different time on stream

Time on stream	Product selectivity in org. phase (%)						α-alkene/total
(h)	Alkanes	Alkenes	Aromatics	Cyclics	Oxygenates compounds		alkenes
6	5.25	39.25	7.99	12.16	35.35		0.31
8	4.30	36.11	7.87	10.29	41.43		0.32

Table C5 GC-MS data obtained from ODH of OA using spent 1.0%V_xO_y/SBA-15 catalyst

Catalyst regenerated	Product selectivity in org. phase (%)						α-alkene/total
cycle	Alkanes	Alkenes	Aromatics	Cyclics	Oxygenates compounds		alkenes
1st regenerated cycle	4.78	39.21	7.56	10.26	38.19		0.32
2nd regenerated cycle	4.86	34.59	3.23	6.62	50.70		0.27
3rd regenerated cycle	4.43	27.16	2.94	6.11	59.36		0.35

VITA

NAME   Nattaporn Chaidherasuwet

DATE OF BIRTH   07 March 1993

PLACE OF BIRTH   Bangkok

HOME ADDRESS   123/67 M.Charisa, Krungthep Kreetha Rd.,

Saphan sung, Bangkok, Thailand, 10250